Research Article

Karolina Młynarczyk*, Beata Podkościelna, Monika Osińska-Jaroszuk, Katarzyna Szałapata and Magdalena Jaszek

Zinc oxide-modified composites as a new antimicrobial coatings for application in biomedical industry – synthesis, thermal stability and antimicrobial properties

https://doi.org/10.1515/pac-2025-0566
Received July 12, 2025; accepted December 2, 2025

Abstract: In recent years, the incidence of hospital-acquired infections has been increasing, which may be caused by the emergence of antibiotic-resistant bacteria. A solution to this problem may be the synthesis of composites containing the addition of compounds with antimicrobial properties, which can form a covering layer. They can limit the spread of bacteria and also reduce the formation of biofilm on the surface of equipment. The optimization of the polymer composition of methacrylate-based composites modified with zinc oxide was identified as the main objective of the research presented in this article. With the use of ATR/FT-IR technique, the structure and qualitative evaluation of the obtained composite materials were performed. The modified composites' thermal resistance and decomposition process were also determined. The antimicrobial potential of the polymers against Gram-negative bacteria (*Pseudomonas aeruginosa* ATCC 27853 and *Escherichia coli* ATCC 25922) and Gram-positive bacteria (*Staphylococcus aureus* ATCC 25923) was determined with a modified disk diffusion method, the serial dilution method and the method with TTC. It was observed that incorporating zinc oxide into the structure of the described polymers significantly increased the antimicrobial potential of the composites and reduced bacterial biofilm formation on their surface. In the case of the effect of composite materials on *P. aeruginosa*, the largest zone of growth inhibition was determined for BPA.DM + AEH + 10 %ZnO, for *E. coli*, the largest zone of growth inhibition was 0.6 cm for BPA.DM + NVP + 10 %ZnO, and for *S. aureus* it was also 0.6 cm for BPA.DM + NVP + 10 %ZnO. Notably, all the materials exhibited antibacterial activity upon contact with bacterial cells. Assessing the percentage of bacterial growth inhibition revealed that had the greatest effect on *P. aeruginosa* was observed with BPA.DM + MMA + 10 % ZnO (49.7 % ± 0.5 % after 12 h and 49.9 % ± 2.1 % after 24 h) and BPA.DM + NVP + 10 % ZnO (62.4 % ± 2.4 % after 12 h). The other materials with the greatest effect on *E. coli* were BPA.DM + AEH (46.0 ± 3.1 % after 12 h and 48.0 ± 0.9 % after 24 h), BPA.DM + AEH + 10 % ZnO (46.7 ± 2.3 % after 12 h) and BPA.DM + NVP (53.5 ± 2.2 % after 24 h). Against *S. aureus*, the highest percentage of growth inhibition was determined for BPA.DM + MMA (56.3 % after 24 h), BPA.DM + HEMA (48.6 % after 24 h), and BPA.DM + NVP (47.9 % after 24 h).

Keywords: (met)acrylates composites; antimicrobial properties; FTIR; polymerization; zinc oxide.

***Corresponding author: Karolina Młynarczyk**, Department of Polymer Chemistry, Maria Curie-Sklodowska University in Lublin, Gliniana 33, Pl-20614, Lublin, Poland, e-mail: karolina.mlynarczyk@mail.umcs.pl. https://orcid.org/0000-0003-3535-5701
Beata Podkościelna, Department of Polymer Chemistry, Maria Curie-Sklodowska University in Lublin, Gliniana 33, Pl-20614, Lublin, Poland. https://orcid.org/0000-0002-0267-5402
Monika Osińska-Jaroszuk, Katarzyna Szałapata and Magdalena Jaszek, Department of Biochemistry and Biotechnology, Institute of Biological Sciences, Maria Curie-Sklodowska University in Lublin, Akademicka 19, Pl-20033, Lublin, Poland. https://orcid.org/0000-0002-3465-0461 (M. Osińska-Jaroszuk). https://orcid.org/0000-0002-0945-0257 (K. Szałapata). https://orcid.org/0000-0003-2609-1820 (M. Jaszek)

Introduction

In recent decades, there has been a significant development of multidrug-resistant microorganisms, representing a significant threat to humans. Multidrug resistance is a phenomenon in which microorganisms show ineffectiveness or resistance to the action of traditionally used drugs with different categories, methods of activity, or different structures.

The World Health Organization, in its studies, in its studies confirms that such micro-organisms can protect themselves against the activity of one or a combination of antimicrobials agents, resulting in the wider spread of pathogens. According to reports, approximately 70 % of micro-organisms indicate resistance to one or more conventionally used pharmaceuticals. As a result, treating infections caused by these microorganisms and stopping their spread with commonly known antibiotics becomes very problematic.[1] The problem concerns not only typical biomedical but also industrial applications, e.g. the formation of bacterial biofilm on the surfaces of industrial devices or everyday objects.[2] Approximately 25 % of hospital infections are caused by antibiotic-resistant bacteria. It is extremely important to restrict the use of antibiotics in order to minimize risks to public health. There are currently numerous studies underway to reverse resistance and prevent the spread of resistant bacteria.[3–6]

A trend in research to solve this problem is the use of nanoparticles characterized by different sizes, shapes, and types of antimicrobial properties. This provides a very promising alternative to the traditional therapies used. Nanoparticles may be prepared using physical as well as chemical and biological methods. The type of method being used depends on the intended function of the chemical compound. Nanoparticles can be a promising alternative against bacteria, fungi, yeast, mold, or multidrug-resistant microorganisms.[7–10]

Modified silver, gold, zinc oxide, iron oxide, or titanium dioxide nanoparticles are used for various antimicrobial applications.[11–15] Their mechanism of activity is based on different theories or approaches. Nanoparticles could adhere to a bacterial cell, which results in changes on its surface. This phenomenon results in a more permeable cell membrane and allows nanoparticles to penetrate the bacterial cell, which in the final stage results in cell death. The second mechanism presented is the production of reactive forms of nanoparticles, which can increase the porosity of the cell membrane. The consequence of such a process is cytoplasmic leakage, resulting also in cell death. Nanoparticles of metals, as well as metal oxides, have an increased affinity for phosphorus and sulfur-containing biomolecules, which are commonly present in the bacterial cell.[16–20]

Zinc oxide is one of the best-known and widely studied in the context of its antimicrobial effect material belonging to the metal oxides group. The conducted studies suggest that it is highly functional, with a wide potential for application in various fields. ZnO nanoparticles of different shapes are characterized by different properties. These include chemical and photochemical stability, anti-inflammatory effects, and beneficial effects on wound healing. In addition, it has the ability to filter ultraviolet radiation, which makes them perfect components of cosmetics or sunscreen lotions. Zinc oxide has very good antibacterial and antifungal properties.[21–25]

Zinc oxide exhibits antimicrobial potential, which is expressed by three mechanisms of activity. The first is the production of reactive oxygen species, which is the result of the semiconducting properties of zinc oxide.[26,27] The other possibility of the total destabilization of microbial membranes consisted of lipids and proteins, which is observed after direct contact of metal nanoparticles with the bacterial cell.[28,29] The last way is the direct reaction of zinc ions released by ZnO in an aqueous environment.[30,31]

The aim of this study was the synthesis of a new composites for biomedical application containing a modifier (in this case zinc oxide) with antimicrobial properties confirmed in the literature. The composites contain bisphenol A glycerolate dimethacrylate as the crosslinking monomer. Synthesis of composites using commercially available monomers with the addition of modifiers possessing antimicrobial properties may bring potential practical benefits. The resulting composites should exhibit good thermal resistance and inhibitory effects when in contact with microorganisms, as well as reducing biofilm formation on their surface. Their use, among other things, as coatings for various surfaces may result in saving time associated with systematic disinfection, as well as reducing the spread of microorganisms. The structure and qualitative evaluation of the obtained composites were conducted with the use ATR-FT/IR spectroscopy. The antimicrobial potential of the estimated materials was

also analyzed. For this purpose, a modification of the disc diffusion method and the method of successive dilutions were used. The possibility of biofilm formation on the surface of the tested composites was also determined.

Materials and methods

Materials

Chemical materials

Bisphenol A glycerolate dimethacrylate (BPA.DM), 1-Vinyl-2-pyrrolidone (NVP), methyl methacrylate (MMA), 2-hydroxyethyl methacrylate (HEMA), 2-ethylhexyl acrylate (AEH) and 2,2-dimethoxy-2-phenylacetophenone (IQ) were purchased from Sigma-Aldrich. Zinc oxide (ZnO) was obtained from Chempur.

Biological materials

In this research, reference strains of bacteria were use: *Escherichia coli* ATCC 25922, *Staphylococcus aureus* ATCC 25923, and *Pseudomonas aeruginosa* ATCC 27853. The biological material used in the study came from the American Type Culture Collection (ATCC) (LGC Standards, Poland).

Preparation of composites

In a 100 ml glass beaker, 8.4g of BPA.DM and 3.6g of one of the comonomers (AEH, MMA, NVP or HEMA) were placed. The mass ratio of comonomers to Bisphenol A glycerolate dimethacrylate was 3:7. The monomer mixture was then transferred to a heating chamber heated to 65 °C for venting. Zinc oxide was added to the mixture in amounts of 1, 5, and 10 wt.% with relation to the weight of the monomer mixture. A composite without a modifier was also prepared as a control sample. UV initiator – IQ was also added in an amount of 1 wt.% for the composite without modifier and containing 1 wt.% ZnO or 2 wt.% for the composite with 5 wt.% ZnO and 3 wt.% for the material with 10 wt.% ZnO. The whole mixture was again mixed thoroughly. The contents of the beaker were transferred to glass moulds which were covered with an anti-stick product and equipped with a Teflon spacer. The moulds were transferred into a chamber equipped with 160 W mercury lamps for 30 min. Then, for whole crosslinking, the molds were transferred to a heating chamber to 85 °C for 4 h. The composite without modifiers was colorless, while those containing zinc oxide were progressively whiter and less transparent with increasing amounts of modifier. In this way, 16 composite materials were obtained. The structure of the monomers used is presented in Fig. 1.

Methods

Chemical methods

ATR/FT-IR (Attenuated Total Reflectance Infrared Spectroscopy) analysis was carried out to verify the chemical structure of obtained materials with using A Bruker FT-IR TENSOR 27 spectrophotometer (Bruker GmbH, Mannheim, Germany). Powdered composite samples were used. Analysis was performed in the wavelength range from 4000 to 600 cm^{-1} in absorbance mode, with 32 scans for each sample.

Using the Netzsch STA 449 F1 Jupiter thermal analyser (Netzsch, Selb, Germany), the thermal stability (TG/DTG) of the composite materials was investigated. A spectroscopic analysis of the gases emitted during the degradation of the samples was also performed. Analysis parameters: temperature range: 25–600 °C, heating rate 10 °C/min, helium atmosphere 20 cm^3/min, sample mass ~15 mg, an empty crucible with Al_2O_3 was used as a

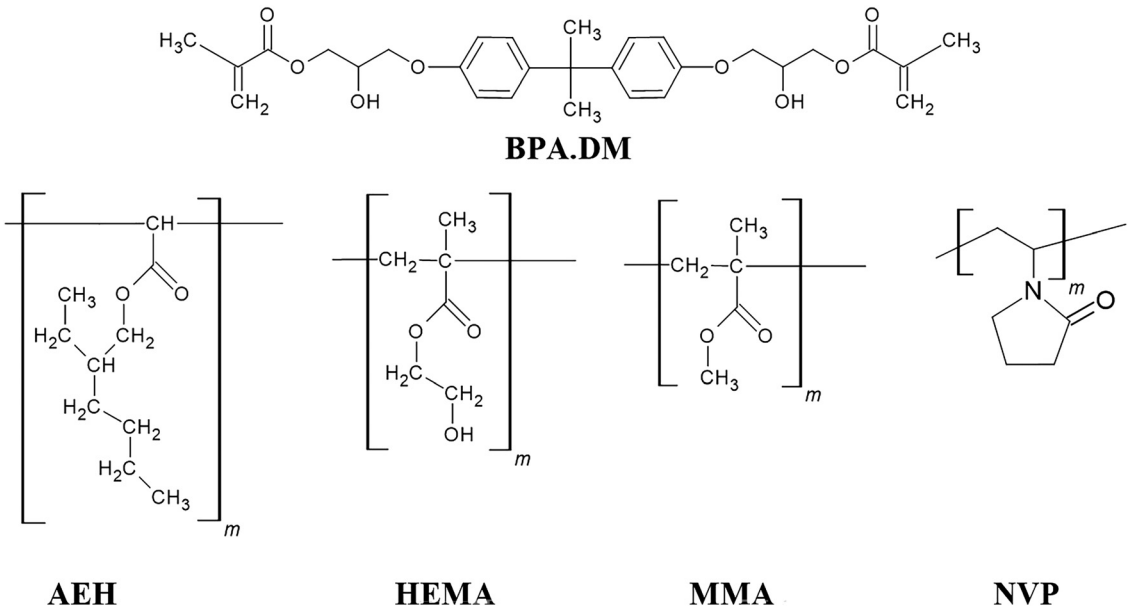

Fig. 1: Chemical structures of monomers [own study].

reference sample. With the use a Netzsch 204 DSC calorimeter (Netzsch, Günzbung, Germany), a differential scanning calorimetry analysis was carried out. Dynamic scans were performed assuming the following analysis parameters: sample mass ~10 mg; temperature range: first stage from 25 to 200 °C, second stage cooling to −50 °C, third stage heating to 550 °C; temperature increase 10 °C/min.2.3.2. Biological tests.

Two strains of Gram-negative bacteria: *E. coli* (ATCC 25922) and *P. aeruginosa* (ATCC 27853) and a Gram-positive bacterial strain: *S. aureus* (ATCC 25923) were used to identify the antimicrobial properties of the composites. All composite fragments were UV-sterilized for 10 min on each side before biological experiments.

Antimicrobial potential tests on agar plates

20 mL of sterile Mueller-Hinton agar medium was placed in Petri plates and allowed to solidify. Overnight bacterial cultures (24 h) were prepared. The concentration of bacteria was 0.5 McFarland. 200 µL of each *inoculum*suspension was transferred on the plates and spread thoroughly over the entire surface of the agar medium. Then composite materials with dimensions 1×1 cm were placed in the middle of the prepared agar plates. The plates with composites were placed in a laboratory incubator (37 °C) for 24 h. Control samples were prepared in an identical procedure using polymers without zinc oxide. Three replicates were performed for each composite material. The materials were then removed from the plate surface and the size of the growth inhibition zone was measured using a manual calliper. Additionally, the plates were archived using GBox (Syngene) scans.

Antimicrobial potential tests in liquid cultures

2.5 mL of Mueller-Hinton liquid medium was placed in sterile 12-well cell culture plates. Young bacterial cultures of *E. coli* (ATCC 25922), *P. aeruginosa* (ATCC 27853), and *S. aureus* (ATCC 25923) were prepared with a bacterial concentration of 0.5 McFarland. Afterward, 100 µL of the appropriate bacterial suspension was added to each well and composites were placed in the wells. A control test was carried out using a culture medium inoculated with bacterial cultures, in which a polymer containing no zinc oxide as a modifier was placed. The initial optical density value was measured on a plate reader (Tecan SPARK) at 600 nm. Then all cultures were incubated in a laboratory incubator at 37 °C, for 12 h. In the next step, 100 µL of fluid from each culture was transferred into a 96-well plate and the optical density at 600 nm was measured. Each sample was performed in triplicate. The process was repeated after 24 h. The % of growth inhibition was determined from the formula: $100\text{-}(OD_p/OD_k) \times 100$ %, where OD_k is the OD of the control sample and OD_p is the OD of the test sample. After measuring optical density,

20 µL of 1 % 2,3,5-triphenyltetrazolium chloride (TTC) solution was added to the wells and placed in a laboratory incubator for 2 h at 37 °C. After this time, the survival of the bacteria was assessed.

Biofilm formation analysis

2.5 mL of Mueller-Hinton liquid medium was placed in sterile 12-well cell culture plates. Young bacterial cultures of *E. coli* (ATCC 25922), *P. aeruginosa* (ATCC 27853) and *S. aureus* (ATCC 25923) were prepared with a bacterial concentration of 0.5 McFarland. The composite plates were thoroughly washed with sterile distilled water to remove all non-adherent bacterial cells. Then composites were transferred to a 12-well plate containing 2.5 mL of Mueller Hinton medium and 100 µL of 1 % TTC solution was added. Three replicates were performed for each composite material. After 24 h of incubation at 37 °C, the formation of bacterial biofilm on the surface of the composites was visually assessed as a phenomenon unfavorable from the practical application point of view. The presence of biofilm on the tested composite material fragments was assessed after thorough rinsing of the materials to remove any unadsorbed bacterial cells. Only after this process were the composite samples placed in a fresh medium enriched with TTC. In this case, the presence of red formazan (the presence of live, metabolically active bacterial cells causes the reduction of TTC to red, insoluble formazan) could only result from the detection of bacterial biofilm. The formation of a biofilm of bacteria indicates the adhesion of bacterial cells to the surface of the composite, which is intended to cover countertops, medical equipment and other elements of the object.

Results and discussion

ATR/FT-IR

Using the ATR/FT-IR attenuated reflection technique, the structure of the obtained composite materials was confirmed. The spectra are summarized in Figs. 2–5. Each spectrum showed a broad absorption band at 3450 cm^{-1}, which was attributed to stretching vibrations of the –OH group. The bands corresponding to 2959 cm^{-1} and 2929 cm^{-1} were attributed to stretching vibrations of the $–CH_3$ and $–CH_2–$ groups. Stretching vibrations originating from the carbonyl group C=O were identified at a wavelength of 1727 cm^{-1}. The bands 1630, 1607, and 1509 cm^{-1} corresponded to stretching vibrations of the aromatic ring $\nu(C_{Ar}C_{Ar})$. At 1459, 1420, and 1385 cm^{-1}, deformation vibrations of the methyl and methylene groups were observed. The bands corresponding to wavelengths 1243, 1164, and 1042 cm^{-1} originated from C–O–C stretching vibrations. Out-of-plane $\gamma(C_{ArH})$

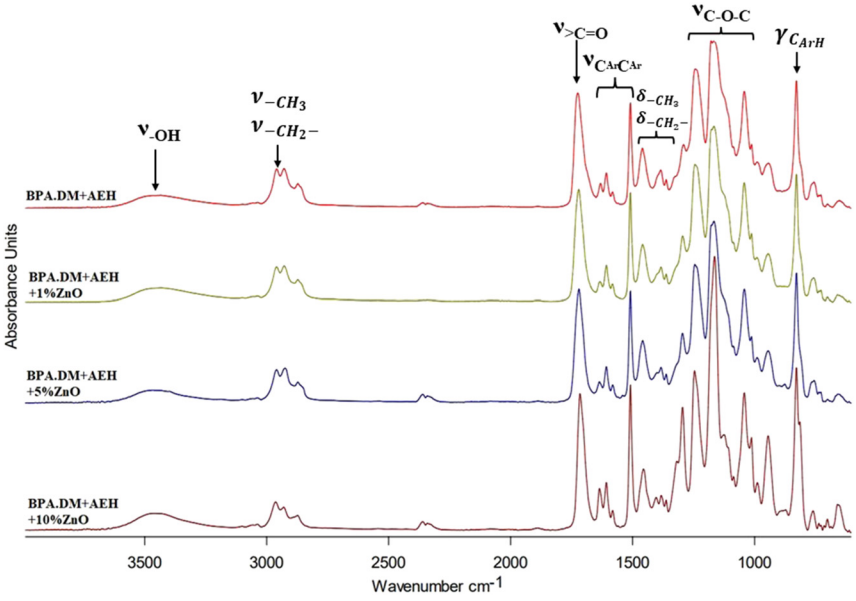

Fig. 2: ATR/FT-IR spectra of AEH-containing composites.

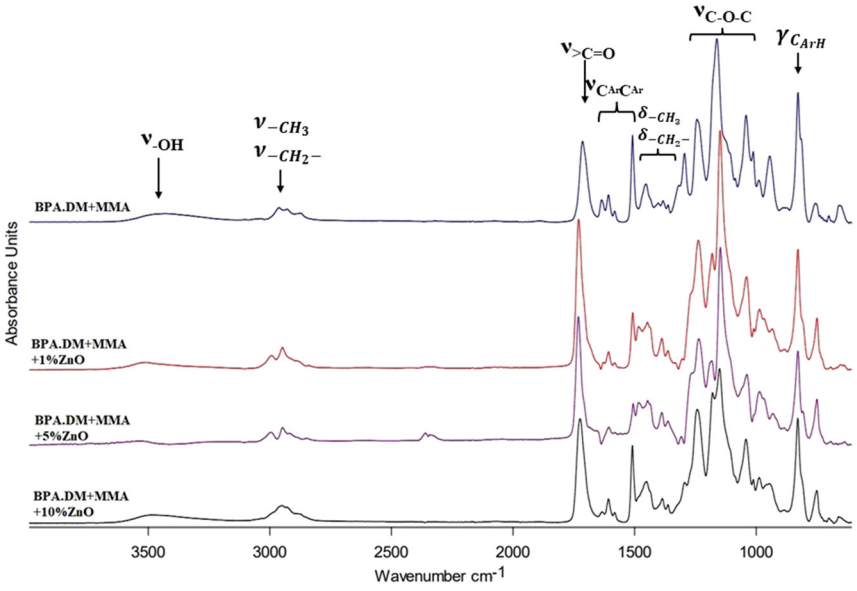

Fig. 3: ATR/FT-IR spectra of MMA-containing composites.

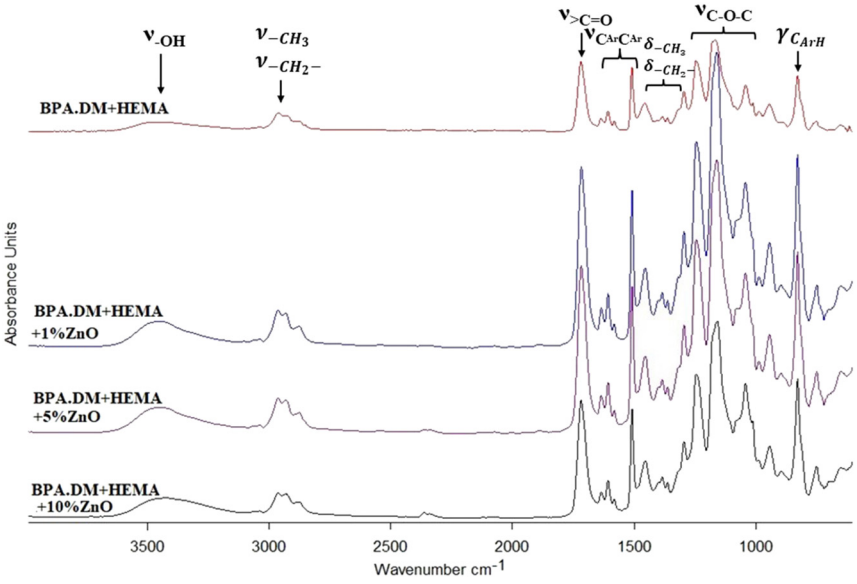

Fig. 4: ATR/FT-IR spectra of HEMA-containing composites.

vibrations from benzene rings occurred at a wavelength of 828 cm^{-1}. A correlation was observed indicating that the intensity of the bands on the ATR/FT-IR spectrum increased with increasing amounts of filler.

The presence of such groups in compounds based on methacrylates but not containing zinc oxide was confirmed by the authors of the work.[32–34] It was observed that increasing the addition of zinc oxide increased the intensity of bands on the spectrum.

TG/DTG analysis

Using thermogravimetric analysis, the thermal properties of composites were confirmed. TG/DTG curves of composites containing AEH are summarized in Figs. 6 and 7 and Table 1. The temperatures associated with a mass loss of 2 %, 5 %, and 50 % ($T_{2\%}$, $T_{5\%}$, $T_{50\,\%}$, respectively) and the temperature of maximum decomposition (T_{max}) were determined for all composites. RM residual mass values were also determined. The AEH-containing

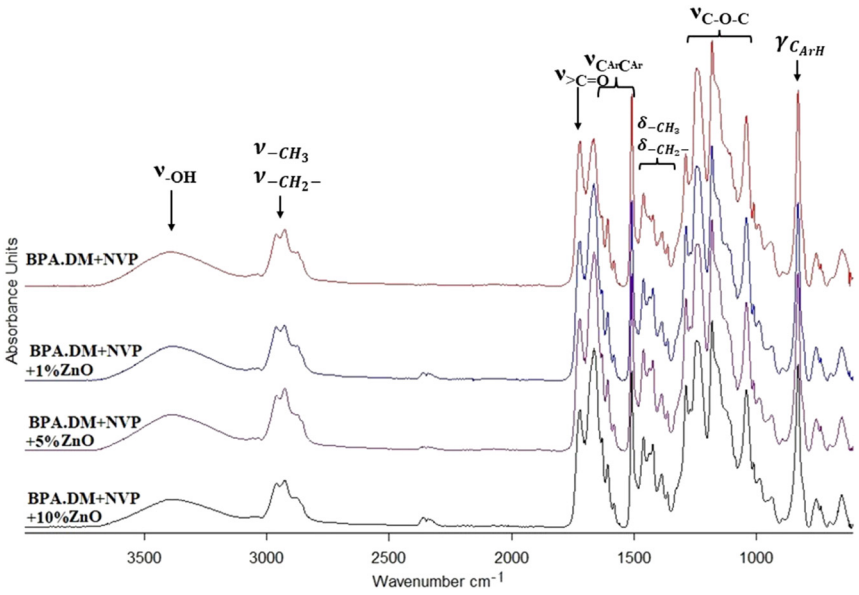

Fig. 5: ATR/FT-IR spectra of NVP-containing composites.

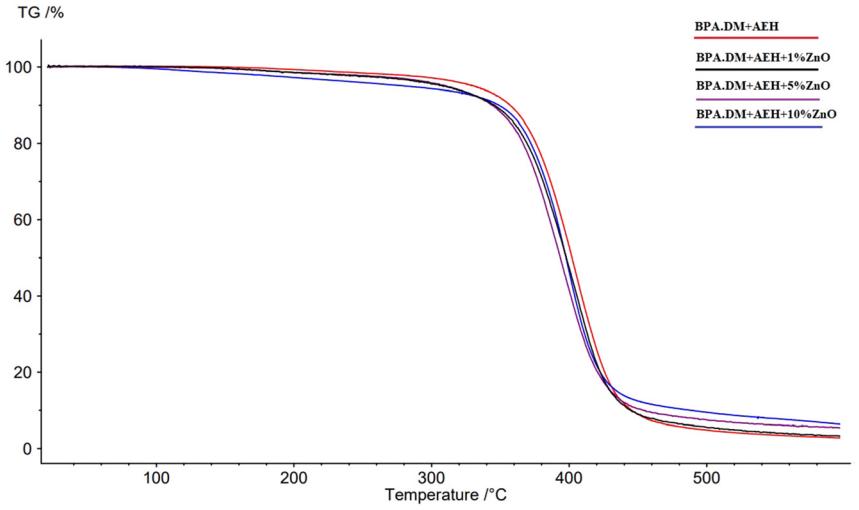

Fig. 6: TG curves of AEH-containing composites.

composites decomposed in a single step, which was further confirmed by the DTG curves. The temperature of the 2 % mass loss oscillated in the range 169.6–272.0 °C. In contrast, the 5 % initial mass loss was in the temperature range of 281.2–330.9 °C. In both examples, the lowest temperature was assigned to the composite modified with 10 % ZnO, while the highest temperature was assigned to the composite containing no modifier. 50 % of the initial mass of the composite decomposed in the range 393.6–402.0 °C, while the maximum decomposition was observed at temperatures 395.4–406.9 °C. The residual mass was between 2.76 and 6.27 %. The higher the modifier concentration in the composite, the higher the residual mass was at the end of the analysis. Thermal tests (TG) on the composite containing AEH modified with zinc oxide were partially published in the monograph chapter.[35]

For MMA-containing composites, a one-step decomposition was observed, as confirmed by the DTG curves (Figs. 8 and 9 and Table 2). The determined temperatures of 2 % initial weight loss ranged from 200.5 to 254.2 °C. 5 % mass loss was observed in the range of 273.0–295.2 °C. 50 % mass loss was determined in the temperature range 388.6–411.0 °C. The temperature of maximum decomposition of the composites varied in the range of 394.1–417.1 °C. The composite BPA.DM + MMA + 5 %ZnO had the lowest temperature values, while the composite containing 10 % zinc oxide had the highest. The residual masses remaining after the combustion process were

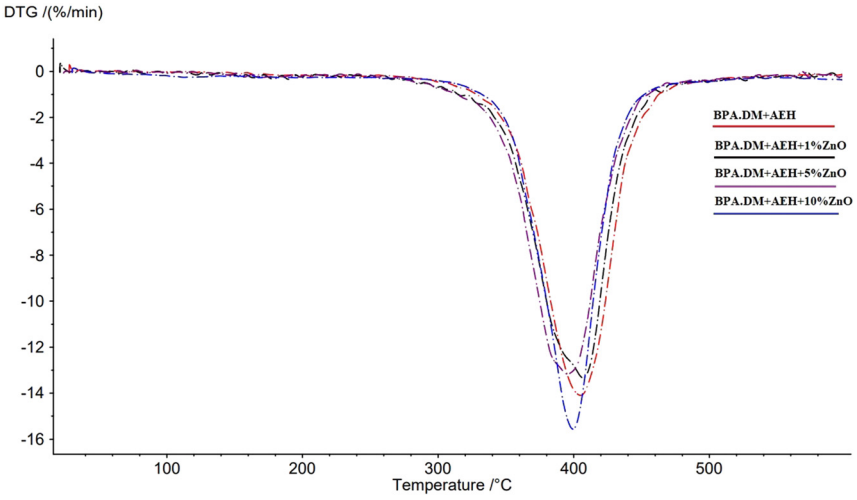

Fig. 7: DTG curves of AEH-containing composites.

Table 1: TG and DTG data for AEH-containing composites.

Composite	$T_{2\,\%;}$ (°C)	$T_{5\,\%}$ (°C)	T_{max} (°C)	$T_{50\,\%}$ (°C)	RM (%)
BPA.DM + AEH	272.0	330.9	405.1	402.0	2.76
BPA.DM + AEH + 1 %ZnO	228.0	308.2	395.4	397.6	3.16
BPA.DM + AEH + 5 %ZnO	236.7	311.2	406.9	393.6	5.35
BPA.DM + AEH + 10 %ZnO	169.6	281.2	399.5	397.7	6.27

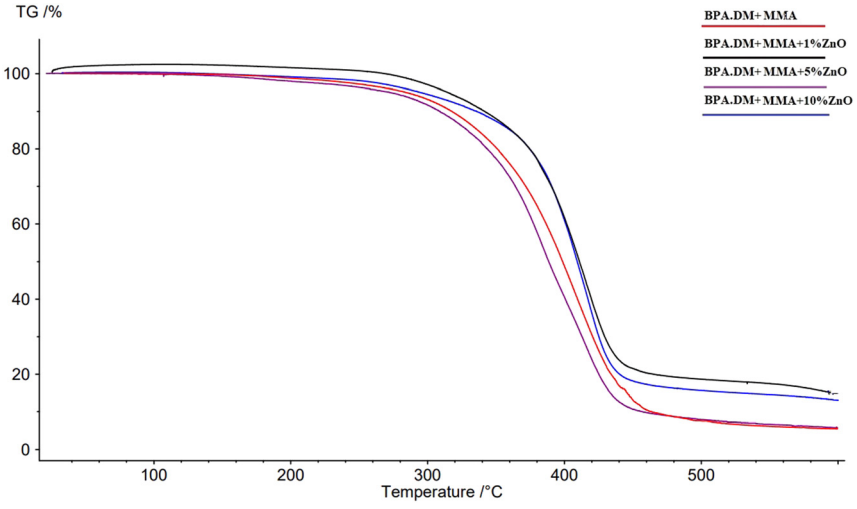

Fig. 8: TG curves of MMA-containing composites.

also determined. These resulted in values of 3.81–7.22 %. The highest value corresponded to the composite BPA.DM + MMA + 10 %ZnO.

TG and DTG graphs, as well as numerical data obtained for composites containing HEMA, are shown in Figs. 10 and 11 and Table 3. The temperatures corresponding to 2 % weight loss of the composites ranged from 183.6 to 261.1 °C and 5 % weight loss from 263.1 to 309.4 °C. 50 % weight loss was determined for temperatures of 390.0–419.0 °C. Maximum decomposition of HEMA-based composite materials took place in the range 396.6–422.5 °C. Residual masses were highest for this type of composite and ranged between 11.32 and 17.66 %.

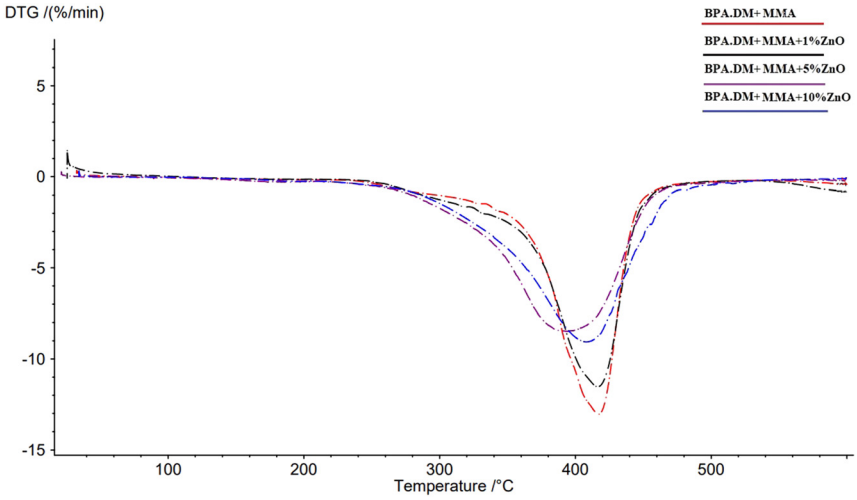

Fig. 9: DTG curves of MMA-containing composites.

Table 2: TG and DTG data for MMA-containing composites.

Composite	$T_{2\,\%}$ (°C)	$T_{5\,\%}$ (°C)	T_{max} (°C)	$T_{50\,\%}$ (°C)	RM (%)
BPA.DM + MMA	231.2	284.8	417.1	398.7	5.48
BPA.DM + MMA + 1 %ZnO	242.5	285.1	416.4	411.0	3.81
BPA.DM + MMA + 5 %ZnO	200.5	273.0	394.1	388.6	5.77
BPA.DM + MMA + 10 %ZnO	254.2	295.2	408.0	409.4	7.22

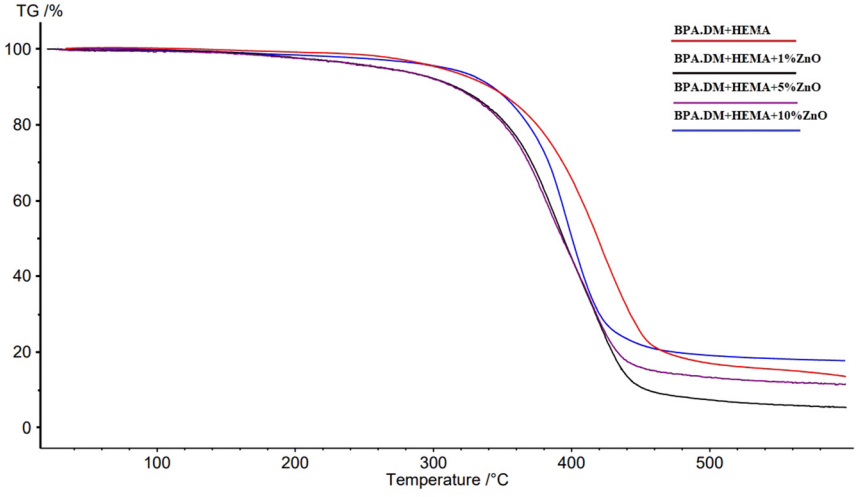

Fig. 10: TG curves of HEMA-containing composites.

For NVP-containing composites, the temperatures associated with 2 % initial weight loss ranged from 139.0 to 185.9 °C, while 5 % weight loss ranged from 186.3 to 237.0 °C. 50 % mass loss was observed in the temperature range of 404.3–421.8 °C Table 4. The temperature of maximum composite decomposition was in the range 409.4–430.9 °C. The composite with no modifier added had the highest temperature, while the composite containing 10 % zinc oxide had the lowest temperature. The residual masses remaining after the combustion process ranged from 5.87 % to 19.51 %. The highest mass was observed for the composite containing 10 % zinc oxide as a modifier. The only composite that degraded in two stages was BPA.DM + NVP + 10 %ZnO, the first degradation temperature was 231.9 °C, and the second 409.4 °C (Figs. 12 and 13).

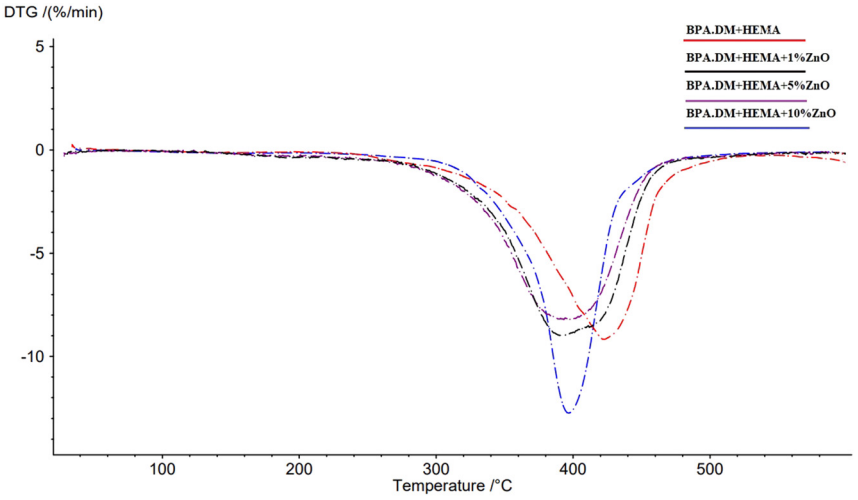

Fig. 11: DTG curves of HEMA-containing composites.

Table 3: TG and DTG data for HEMA-containing composites.

Composite	$T_{2\,\%}$ (°C)	$T_{5\,\%}$ (°C)	T_{max} (°C)	$T_{50\,\%}$ (°C)	RM (%)
BPA.DM + HEMA	261.1	305.2	422.5	419.0	13.43
BPA.DM + HEMA + 1 %ZnO	259.8	292.1	399.5	390.0	11.32
BPA.DM + HEMA + 5 %ZnO	183.6	263.1	396.6	393.1	11.47
BPA.DM + HEMA + 10 %ZnO	223.6	309.4	396.8	400.3	17.66

Table 4: TG and DTG data for NVP-containing composites.

Composite	$T_{2\,\%}$ (°C)	$T_{5\,\%}$ (°C)	T_{max1} (°C)	Δm_1 [%]	T_{max2} (°C)	Δm_2 [%]	$T_{50\,\%}$ (°C)	RM (%)
BPA.DM + NVP	185.9	215.9	–	–	430.9	86.34	421.8	13.66
BPA.DM + NVP + 1 %ZnO	149.4	210.4	–	–	415.7	94.13	409.4	5.87
BPA.DM + NVP + 5 %ZnO	154.3	237.0	–	–	411.6	89.11	404.3	10.89
BPA.DM + NVP + 10 %ZnO	139.0	186.3	231.9	17.55	409.4	62.94	404.9	19.51

The least thermal resistant composite was BPA.DM + NVP + 10 %ZnO, for which the temperature related to the loss of 2 % of initial weight was 139.0 C. The most thermally resistant was BPA.DM + AEH, for which the temperature related to the loss of 2 % of initial weight was 272.0 C. No conclusive correlation was observed between the zinc oxide content and the thermal resistance of the tested material. The main effect on the thermal resistance of the materials was shown by the comonomer used.

TG-FTIR analysis

For the AEH-containing composite as an active diluent, maximum decomposition temperature were observed at 405.1 °C (BPA.DM + AEH – Fig. 14) and 399.5 °C (BPA.DM + AEH + 10 %ZnO – Fig. 15). The gases evolved at this temperature correspond to the temperature at the emission maximum. The spectra of gaseous decomposition products emitted during heating showed the presence of water molecules (stretching vibrations of the–OH group 3500–4000 cm^{-1}, deformation vibrations of the –OH group 1300–1800 cm^{-1}). In addition, bands originating from carbon dioxide (stretching vibrations 2310–2350 cm^{-1} and deformation vibrations 600–700 cm^{-1}). A band

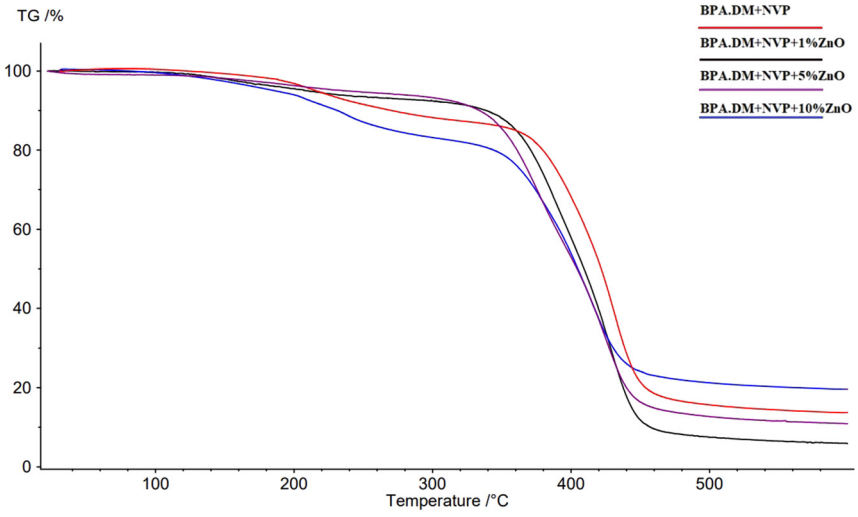

Fig. 12: TG curves of NVP-containing composites.

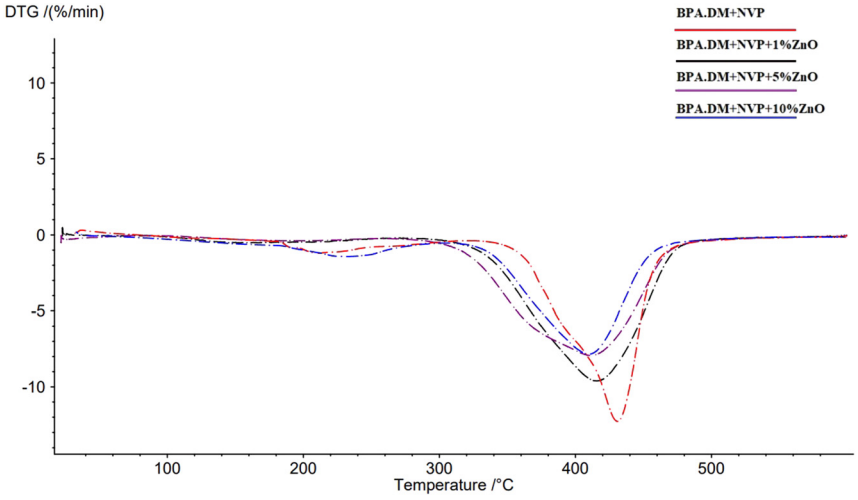

Fig. 13: DTG curves of NVP-containing composites.

originating from the carbonyl group (1750–1790 cm^{-1}), as well as a bands from stretching vibrations of the methyl and methylene groups (2970 cm^{-1}, 2885 cm^{-1}) were visible. The bands observed in the range 1505–1603 cm^{-1} corresponded to symmetric and asymmetric stretching vibrations of the aromatic ring. In addition, a band originating from Ar and Ar-H deformation vibrations was observed around 828 cm^{-1}. Bands at 1120–1180 cm^{-1} corresponded to the stretching vibrations of C–O–C ester groups.

Figures 16–21 show the spectroscopic analysis of the gases released during the heating of the other composite materials. A similar pattern of material decomposition reactions is observed.

DSC analysis

The curves of the DSC for composites containing AEH as a comonomer were quite similar (Fig. 22). One main endothermic effect was visible in the temperature range of 366–399 °C. This effect was most probably corresponded to the thermal decomposition of the samples. The highest temperature was observed for the composite that contained no modifier. As the amount of zinc oxide increased, the temperature value at which decomposition of the sample occurred gradually decreased.

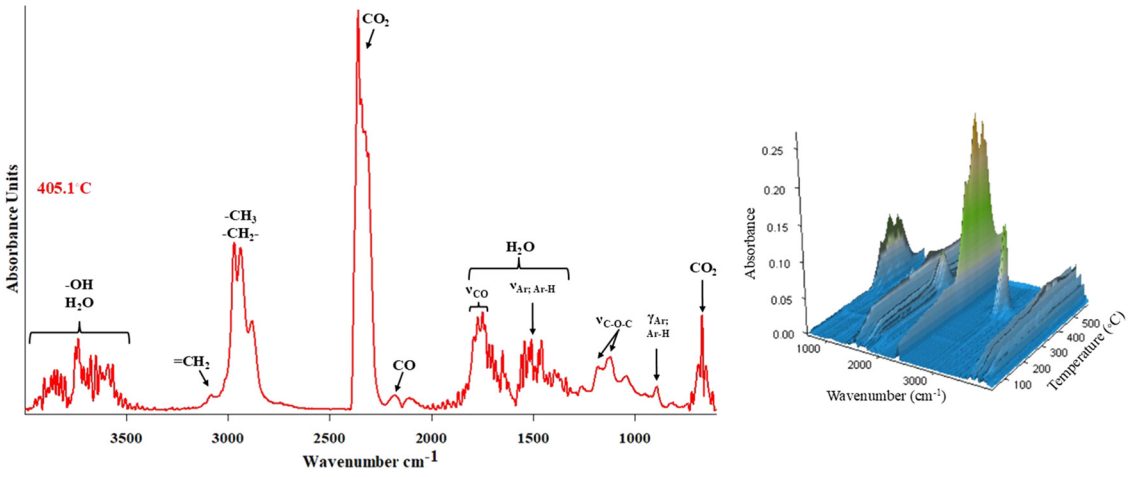

Fig. 14: ATR/FT-IR spectra and 3D diagram of FT-IR absorption of evolved gases for BPA.DM + AEH at the maxima of decomposition.

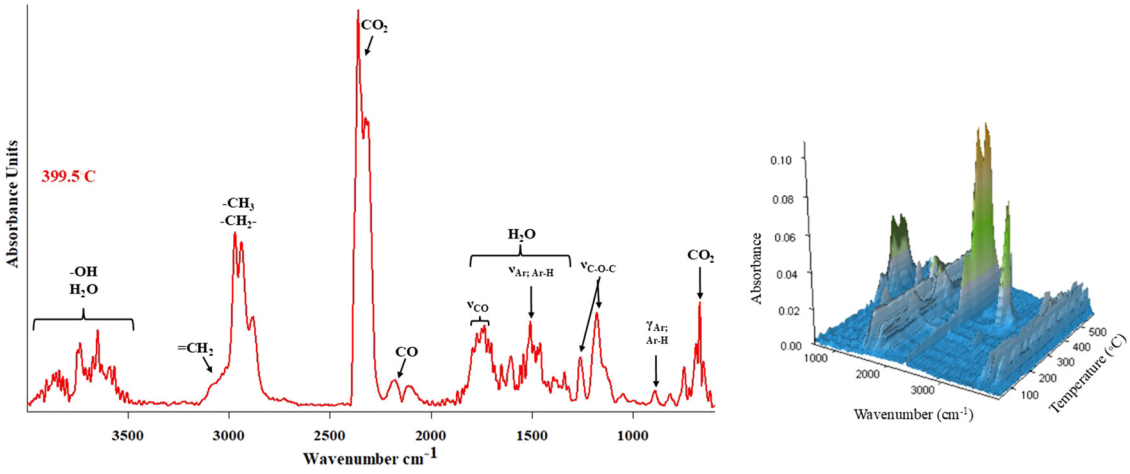

Fig. 15: ATR/FT-IR spectra and 3D diagram of FT-IR absorption of evolved gases forBPA.DM + AEH + 10 %ZnO at the maxima of decomposition.

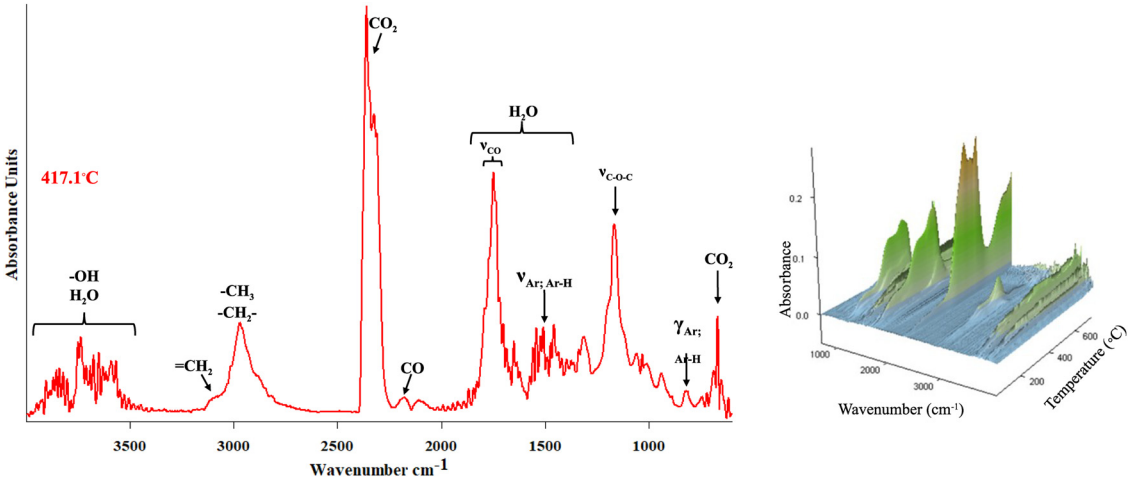

Fig. 16: ATR/FT-IR spectra and 3D diagram of FT-IR absorption of evolved gases forBPA.DM + MMA at the maxima of decomposition.

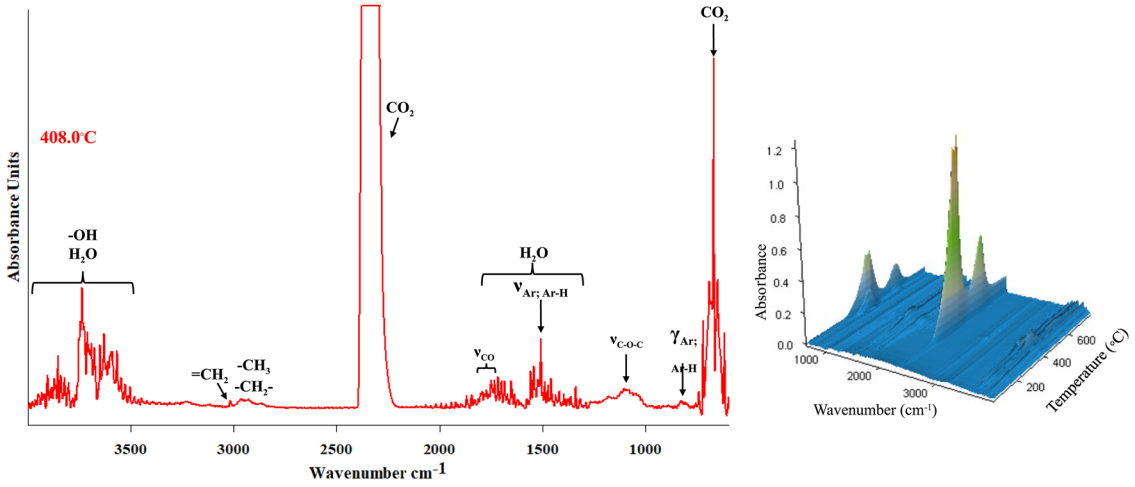

Fig. 17: ATR/FT-IR spectra and 3D diagram of FT-IR absorption of evolved gases forBPA.DM + MMA + 10 %ZnO at the maxima of decomposition.

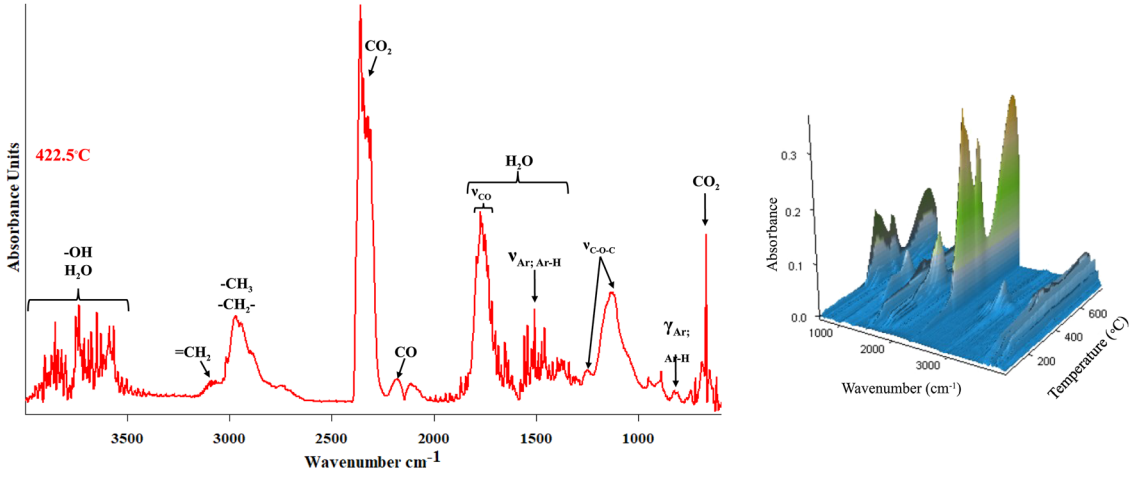

Fig. 18: ATR/FT-IR spectra and 3D diagram of FT-IR absorption of evolved gases forBPA.DM + HEMA at the maxima of decomposition.

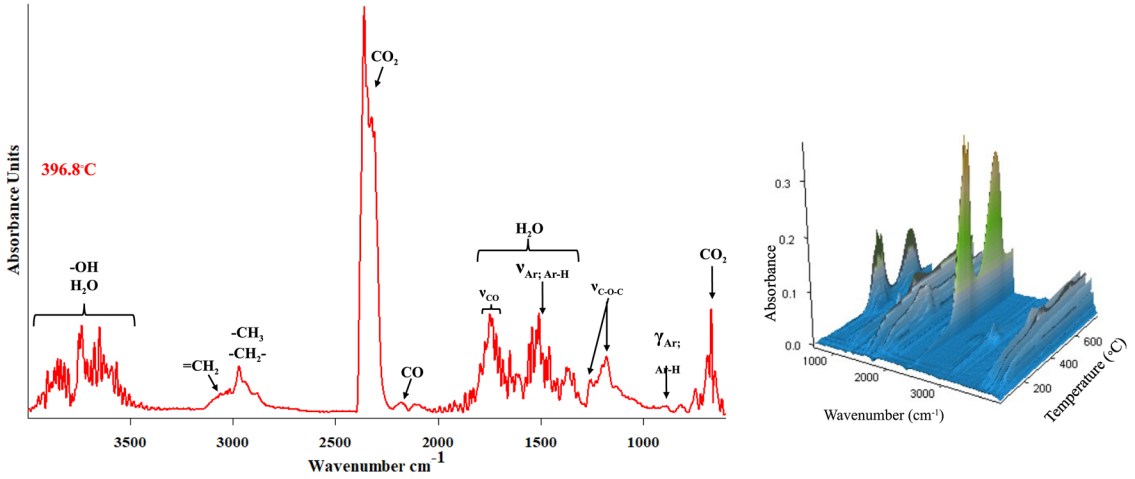

Fig. 19: ATR/FT-IR spectra and 3D diagram of FT-IR absorption of evolved gases forBPA.DM + HEMA + 10 %ZnO at the maxima of decomposition.

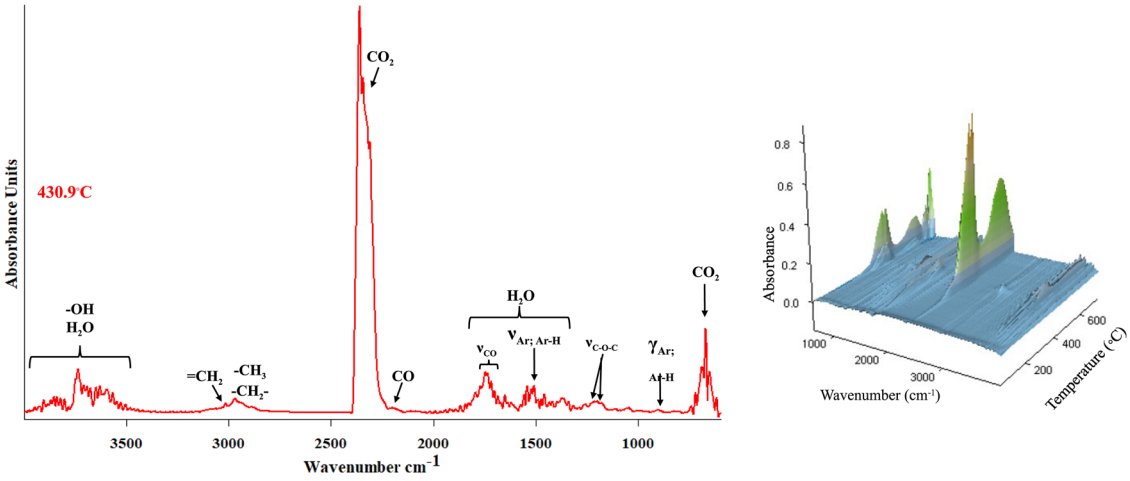

Fig. 20: ATR/FT-IR spectra and 3D diagram of FT-IR absorption of evolved gases for BPA.DM + NVP at the maxima of decomposition.

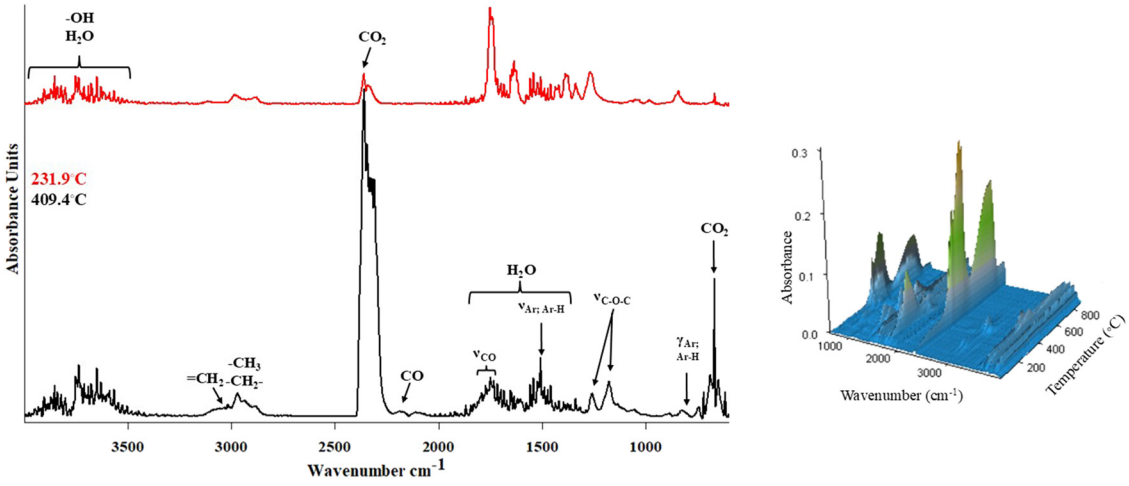

Fig. 21: ATR/FT-IR spectra and 3D diagram of FT-IR absorption of evolved gases for BPA.DM + NVP + 10 %ZnO at the maxima of decomposition.

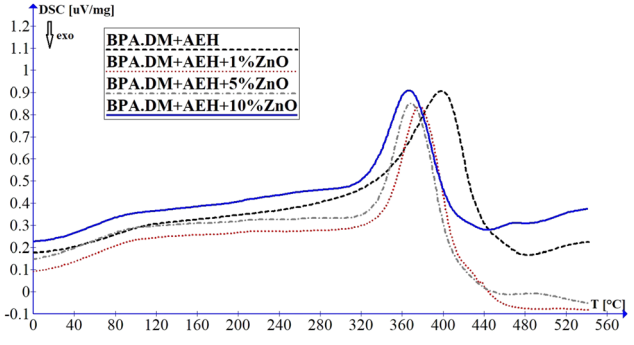

Fig. 22: DSC curves of AEH-containing composites.

For composites containing MMA (Fig. 23), the addition of zinc oxide increased the decomposition temperature of composites. In the DSC curves, as above, one endothermic effect was observed, indicating sample decomposition. For the composite without the modifier, the decomposition temperature was 364 °C. The addition of 1 and

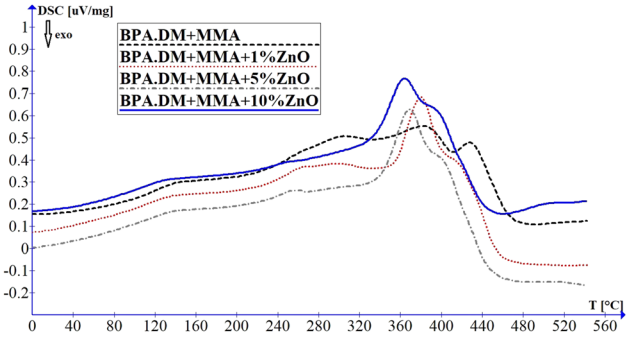

Fig. 23: DSC curves of MMA-containing composites.

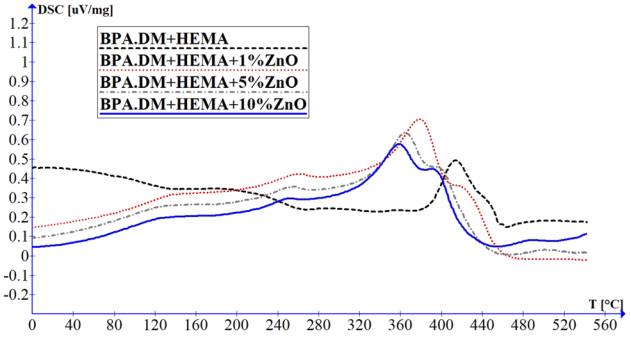

Fig. 24: DSC curves of HEMA-containing composites.

10 % ZnO increased the decomposition temperature value (to 379 °C and 383 °C, respectively), while the 5 % addition slightly increased this value (to 369 °C).

A similar result as AEH materials was observed for composites containing HEMA (Fig. 24). The highest decomposition temperature was recorded for the material that contained no modifier (413 °C). On the other hand, the higher the zinc oxide addition, the decomposition temperature of the material (for BPA.DM + HEMA + 10 % ZnO – 359 °C) was lower.

The curves were slightly different for materials containing NVP (Fig. 25). The first thermal effect was observed in the temperature range of 356–360 °C and could probably came from the decomposition of the composite material. A second effect of lower intensity was observed in the temperature range of 484–500 °C and was attributed to the probable decomposition of the modifier here.

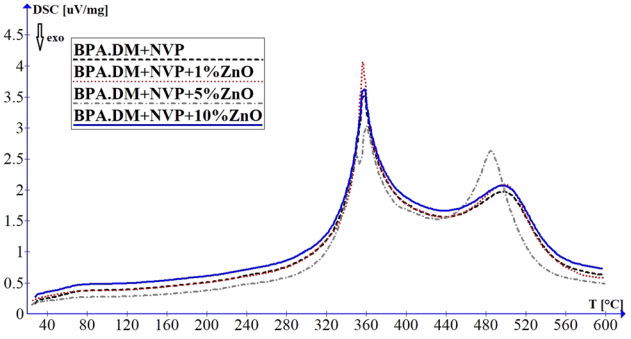

Fig. 25: DSC curves of NVP-containing composites.

Determination of antimicrobial activity

All antimicrobial activity tests for composites modified with the addition of zinc oxide were examined against selected strains of Gram-negative (*P. aeruginosa* and *E. coli*) and Gram-positive (*S. aureus*) pathogenic bacteria.

Antimicrobial potential tests on agar plates

In the first instance, tests were carried out using a modified disk-diffusion method. Results from the modification of the disk-diffusion method on the composite containing AEH modified with zinc oxide for the bacteria *P. aeruginosa* and *S. aureus* were partially published in the monograph chapter.[35] As was presented in the Table 5, all composites containing AEH exhibited visible antimicrobial activity in contact with bacterial cells. For composites that did not contain a modifier, growth inhibition was evident under the composite pieces. No characteristic biofilm formation was observed on the surface on which the composite was placed. This indicated no bacterial growth under the surface of the presented polymer probes. For the material containing 10 % ZnO, a diffusion zone (zone of growth inhibition) was visible in the case of *P. aeruginosa* and *E. coli* strains, indicating the release of the modifying agent into the substrate. The growth in the inhibition zone was 1.4 cm in *P. aeruginosa* case and 0.5 cm in *E. coli*. For *S. aureus* the inhibitory effect of the composite was observed only in the contact area under the composite pieces.

For the composite containing MMA as a solvent, a similar relationship was observed (Table 6). Composites that did not contain a modifier presented antimicrobial activity in the area of direct contact with the composite material. For the zinc oxide-modified composite, a bacterial growth inhibition zone for *P. aeruginosa* (0.5 cm) and *E. coli* (0.3 cm) was identified. In the case of *S. aureus*, an antimicrobial effect was observed at the direct contact area of the composite material.

In the case of both composites containing HEMA (Table 7), an inhibitory effect on the growth of the pathogenic microorganisms tested was evident on the surface on which the composites were placed. Furthermore, in the case of the composite modified with 10 % zinc oxide, zones of growth inhibition were also evident for all bacterial cells tested. For *P. aeruginosa* and *E. coli*, the inhibition zone was 0.4 cm, while for *S. aureus* it was 0.1 cm.

Table 5: Antimicrobial activity of control-based and zinc oxide-containing AEH composites against pathogenic bacteria: *P. aeruginosa, E. coli* and *S. aureus* using the modified disk-diffusion method. The pieces of composite were lifted to show the growth inhibition zones of bacteria under the sample. Growth inhibition zones are given in cm.

Microorganism/composite	*P. aeruginosa*	*E. coli*	*S. aureus*
BPA.DM + AEH	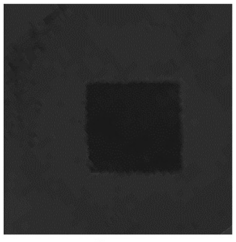 0 cm	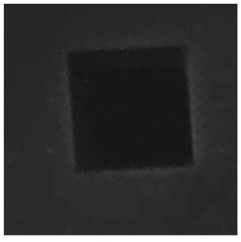 0 cm	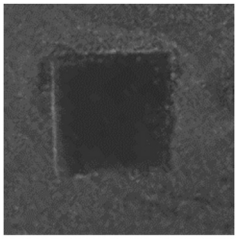 0 cm
BPA.DM + AEH + 10 %ZnO	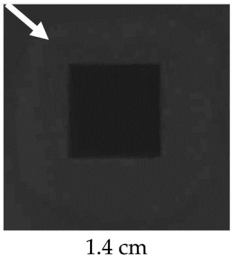 1.4 cm	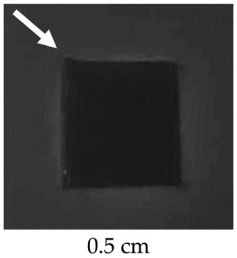 0.5 cm	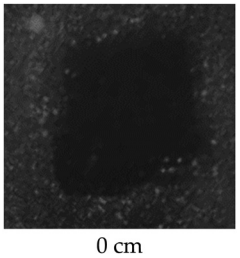 0 cm

Table 6: Antimicrobial activity of control-based and zinc oxide-containing MMA composites against pathogenic bacteria: *P. aeruginosa, E. coli* and *S. aureus* using the modified disk-diffusion method. The pieces of composite were lifted to show the growth inhibition zones of bacteria under the sample. Growth inhibition zones are given in cm.

Microorganism/composite	*P. aeruginosa*	*E. coli*	*S. aureus*
BPA.DM + MMA	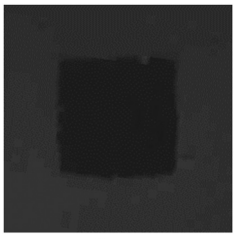 0 cm	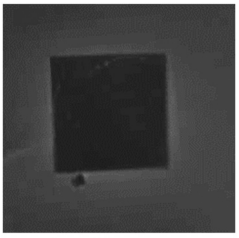 0 cm	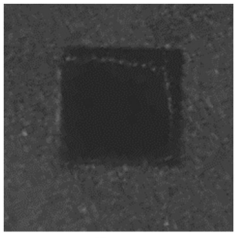 0 cm
BPA.DM + MMA + 10 %ZnO	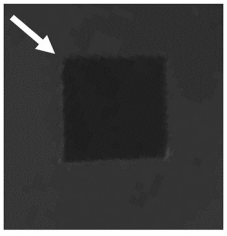 0.5 cm	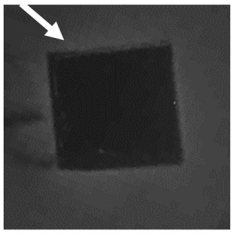 0.3 cm	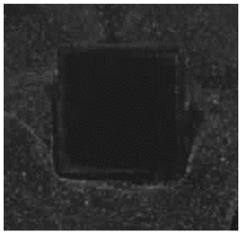 0 cm

Table 7: Antimicrobial activity of control-based and zinc oxide-containing HEMA composites against pathogenic bacteria: *P. aeruginosa, E. coli* and *S. aureus* using the modified disk-diffusion method. The pieces of composite were lifted to show the growth inhibition zones of bacteria under the sample. Growth inhibition zones are given in cm.

Microorganism/composite	*P. aeruginosa*	*E. coli*	*S. aureus*
BPA.DM + HEMA	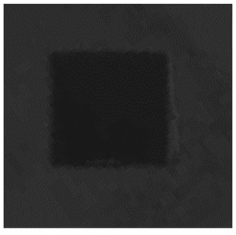 0 cm	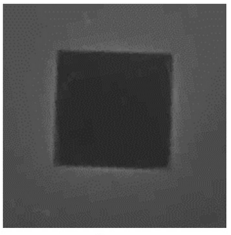 0 cm	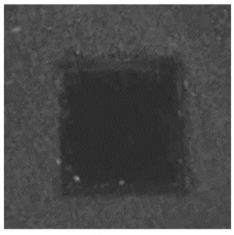 0 cm
BPA.DM + HEMA + 10 %ZnO	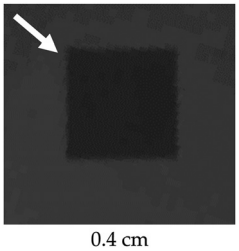 0.4 cm	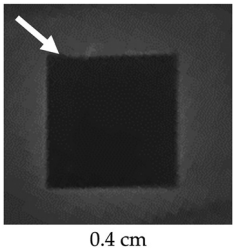 0.4 cm	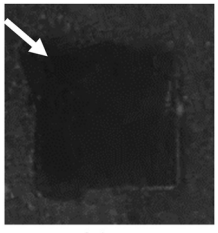 0.1 cm

Similar to the composites shown previously, the NVP-containing materials exhibited antimicrobial activity in the area of direct contact with bacteria. Modification of the materials with 10 % zinc oxide resulted with the observation of growth inhibition zones around the surface where the composite fragment was located. For *P. aeruginosa*, the inhibition zone was 0.7 cm, while for *E. coli* and *S. aureus* it was 0.6 cm. Results from the

Table 8: Antimicrobial activity of control-based and zinc oxide-containing NVP composites against pathogenic bacteria: *P. aeruginosa, E. coli* and *S. aureus* using the modified disk-diffusion method. The pieces of composite were lifted to show the growth inhibition zones of bacteria under the sample. Growth inhibition zones are given in cm.

Microorganism/composite	*P. aeruginosa*	*E. coli*	*S. aureus*
BPA.DM + NVP	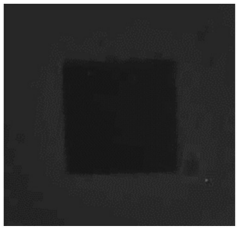 0 cm	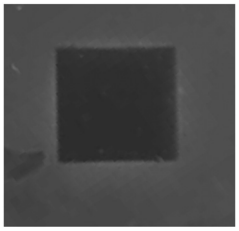 0 cm	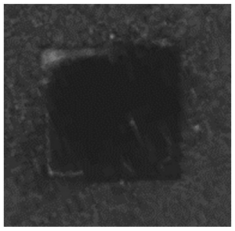 0 cm
BPA.DM + NVP + 10 %ZnO	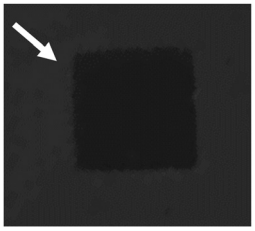 0.7 cm	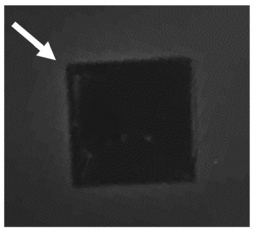 0.6 cm	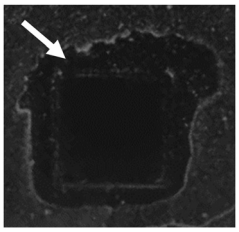 0.6 cm

modification of the disk-diffusion method on the zinc oxide-modified NVP-containing composite for the bacteria *P. aeruginosa*, *E. coli* and *S. aureus* were partially published in the monograph chapter (Table 8).[36]

In the case of newly synthetized composites presented here all of them showed visible antimicrobial activity in contact with bacterial cells. For the composite materials zinc oxide-modified composites, the largest growth inhibition zones were observed in contact with *P. aeruginosa* and ranged from 0.4 cm to 1.4 cm. For *E. coli*, the largest measured zone was 0.6 cm (BPA.DM + NVP + 10 %ZnO) and the smallest was 0.3 cm (BPA.DM + MMA + 10 % ZnO). For *S. aureus* strain, growth inhibition zones were only visible for BPA.DM + HEMA + 10 %ZnO (0.1 cm) and BPA.DM + NVP + 10 %ZnO (0.6 cm). The obtained results may indicate the probable release of zinc oxide, which is a component of the described polymers, into the culture media and a direct impact on the growing bacterial cells. This fact confirms the antiseptic properties of ions described in the literature.[37–39] A similar effect was observed in the previous study published by Młynarczyk et al.[40] when the antimicrobial potential of composites based on bisphenol A diacrylate with 5 % zinc oxide addition was determined. It was indicated that the inhibition zones for *E. coli* were between 0.3 and 0.7 cm, while for *S. aureus* they were 0.2–0.6 cm. Tests conducted on zinc oxide-impregnated paper discs performed by Gunalan et al.[41] indicated that growth inhibition zones ranged from 1.0 to 1.6 cm[42] in their study, presented research confirming that nanocomposites containing ZnO and chitosan showed greater antimicrobial activity against Gram-negative bacteria than Gram-positive bacteria. In experiments performed by Cheknev team[43] the authors indicated zinc oxide did not show antimicrobial properties against *S. aureus*. In the work Ibrahem et al.[44] it was shown zinc oxide nanoparticles caused the formation of growth inhibition zones for *P. aeruginosa* (2.5 cm) and *S. aureus* (2.8 cm). These results were similar to a study published by M. Yousef and N. Danial.[45]

Antimicrobial potential tests in liquid cultures

Using the calculation formula presented in Section 2.3.2 of Materials and methods, the percentage of bacterial growth inhibition was determined 12 and 24 h after the initiation of growth (Table 9). Grey color indicates bacterial growth inhibition higher than 45.0 %. For *P. aeruginosa*, it was observed that for most composites the bacterial growth inhibition value increases after 24 h. The exceptions were BPA.DM + AEH + 10 %ZnO and

BPA.DM + NVP + 10 %ZnO, where the value after 24 h is lower than after 12 h of culture. A similar relation was observed for *S. aureus*. Only in the case of BPA.DM + HEMA + 10 %ZnO and BPA.DM + NVP + 10 %ZnO a slight reduction in the percentage of growth inhibition was determined. In the case of *E. coli*, it was observed for BPA.DM + AEH, BPA.DM + HEMA and BPA.DM + NVP that the percentage growth inhibition value of the bacteria increases after 24 h, whereas the value decreases for the other composite materials. For *P. aeruginosa*, the highest percentage growth inhibition values were observed for BPA.DM + MMA after 24 h (73.4 ± 0.9 %) and BPA.DM + NVP (59.4 ± 2.2 %). For *E. coli*, the values were higher after 12 h of culture, with the highest value for BPA.DM + AEH + 10%ZnO (46.7 ± 2.3 %). For *S. aureus*, the highest % of bacterial growth inhibition was calculated for BPA.DM + HEMA (48.6 ± 1.2 %) and BPA.DM + NVP (47.9 ± 2.0 %). These values were observed 24 h after the start of culture. Interestingly similar values for *P. aeruginosa* were shown in the work of Chitra et al.[46] In the work of Li et al.,[47] antimicrobial PVC films coated with ZnO powder were shown to have antimicrobial activity against Gram-positive and Gram-negative bacteria. The larger the contact area and the higher the ZnO concentration, the antimicrobial activity of the ZnO nanoparticles increased accordingly. The authors determined the growth inhibition zone of *E. coli* and *S aureus* using ZnO-coated film and PVC film as a control. It was observed that by increasing the concentration of ZnO nanoparticles from 93.75 μg/cm^2 to 187.50 μg/cm^2 the inhibition zones increased too – by 2.3 mm for *E. coli* and 2.0 mm for *S. aureus*, respectively. These results allowed the authors to conclude that Gram-negative bacteria, such as *E. coli*, show greater resistance to the antimicrobial effect of zinc oxide nanoparticles than Gram-positive bacteria, such as *S. aureus*, or *B. atrophaeus*. The differences in this effect were explained by differences in the structure and thickness of the cell wall between bacteria. In the case of the cell wall of Gram-positive bacteria, the normally thick homogeneous cell wall consists mainly of peptidoglycan, which accounts for almost 80 % of its structure. In Gram-negative bacteria, on the other hand, this layer makes up about 10 % of the cell wall. The peptidoglycan amount, as well as the structure of the external wall, allows protection and also determines sensitivity to compounds with antimicrobial properties. On the other hand,[48] presented that, more than 90 % inhibition of bacterial growth was obtained using zinc oxide nanoparticles against *E. coli* and *S. aureus*. The authors used zinc oxide nanoparticles synthesized in diethylene glycol substrates. Luria-Bertani medium containing ZnO nanoparticles was used, on which cultures of *E. coli* and *S. aureus* were inoculated. After a 12-hour incubation at 37 °C, colony-forming units (CFU) were enumerated. ZnO concentrations greater than 3.4 mM were shown to inhibit the growth of *E. coli*, while concentrations greater than 1 mM prevented the growth of *S. aureus*. The number of viable bacterial cells was shown to be reduced to less than 90 % of the initial number of CFU per mL after 12 h, and the complete absence of cells was demonstrated after 24 h.

Table 9: Analysis of bacterial cell growth inhibition [%] in liquid cultures after 12 and 24 h of incubation in the presence of control-based and zinc oxide-modified composites containing AEH, MMA, HEMA and NVP as solvent using the serial dilution method. Data presented as mean value with SD. All experiments were performed in triplicates.

	P. aeruginosa		*E. coli*		*S. aureus*	
	After 12 h	**After 24 h**	**After 12 h**	**After 24 h**	**After 12 h**	**After 24 h**
BPA.DM + AEH	39.6 ± 1.6	40.5 ± 2.0	46.0 ± 3.1	48.0 ± 0.9	32.4 ± 1.4	43.6 ± 1.3
BPA.DM + AEH + 10 %ZnO	36.8 ± 1.1	36.0 ± 1.3	46.7 ± 2.3	14.6 ± 0.4	18.1 ± 0.7	22.3 ± 0.2
BPA.DM + MMA	5.5 ± 0.9	73.4 ± 0.9	39.5 ± 0.4	33.4 ± 1.2	7.5 ± 0.2	56.3 ± 0.4
BPA.DM + MMA + 10 %ZnO	49.7 ± 0.5	49.9 ± 2.1	39.5 ± 1.1	13.4 ± 0.3	4.8 ± 0.5	19.6 ± 0.7
BPA.DM + HEMA	22.5 ± 1.4	40.7 ± 1.8	34.6 ± 0.6	36.9 ± 0.4	18.3 ± 0.6	48.6 ± 1.2
BPA.DM + HEMA + 10 %ZnO	22.2 ± 0.7	32.0 ± 0.4	40.0 ± 1.0	16.9 ± 1.1	18.0 ± 1.1	17.1 ± 1.1
BPA.DM + NVP	17.8 ± 1.9	59.4 ± 2.2	40.0 ± 0.0.7	53.5 ± 2.2	29.4 ± 2.0	47.9 ± 2.0
BPA.DM + NVP + 10 %ZnO	62.4 ± 2.4	24.4 ± 0.6	44.6 ± 1.1	3.5 ± 0.3	24.1 ± 1.1	19.6 ± 0.4

Bacteria survival after contact with composite samples

The conversion of 2,3,5-triphenyltetrazolium chloride (TTC) to insoluble red 1,3,5-triphenylformazane (TPF) depends on the metabolic activity of the bacteria. This method makes it possible to determine the concentration of viable bacterial cells in solutions.[49] Using the method with TTC, the survival rate of bacteria after contact with the composite materials was determined. The results obtained are summarized in Table 10. The presence of red-colored formazan was indicative of the presence of alive bacterial cells in the culture medium and the intensity of its colour is directly proportional to the number of living cells present in the suspension. For *P. aeruginosa*, no alive bacterial cells were observed. For both control and zinc oxide composites, no red coloring was visible in the wells of the culture plate. For *E. coli*, red staining was only visible for composites that did not contain the modifier. However, it should be noted that this staining was much less intense than for the bacterial growth control. For *S. aureus*, alive bacterial cells were present in all wells of the culture plate. The concentration of red formazan was less intense when the bacteria were in contact with composites that contained the modifier – zinc oxide.

The result confirms that both composites containing no modifier and those containing zinc oxide significantly reduce the number of viable bacterial cells in the solution. This was confirmed by the color of the bacterial suspensions in the wells, which contained no red staining. This is particularly noticeable for *P. aeruginosa*. For both *E. coli* and *S. aureus*, the color of all suspensions was less intense than the control sample. This allows us to conclude that the presence of zinc oxide in the composite material allows a significant reduction in the metabolism of the bacterial cells and thus limits their viability.[50] showed that the addition of zinc oxide to cotton-polyester fabrics significantly reduces the viability of *E. coli* and *Micrococcus luteus* bacteria. The presence of zinc oxide reduces the number of viable bacteria to approximately 70 %.[51] described the use of TTC to evaluate the antipathogenic activity of chitosan against *Salmonella typhimurium* and *S. aureus*. They presented the inhibitory concentration of chitosan was lower for *S. typhimurium* than for *S. aureus*, which may be due to the lover activity of Gram-negative bacteria to reduce TTC to red formazan than for Gram-positive bacteria.

Biofilm formation analysis

Using the method with TTC as a reaction substrate, the possibility of bacterial biofilm formation on the surface of the tested composite materials was also determined Table 11. It was observed that the 10 % addition of zinc oxide to the composite significantly reduced the presence of the bacterial biofilm on the surface of the tested samples in comparison to control samples. In the case of *P. aeruginosa*, a small amount of biofilm was visible for BPA.DM + AEH at the edges of the polymer's samples, and this may be the consequence of sharp edges of composites after the cutting process. Sharp and uneven edges promote increased adhesion of bacterial cells to abiotic surfaces. For all other samples, very small red spots were visible, or the color was not noticeable at all. For *E. coli*, a fairly significant red staining was visible on the surface of the composites containing NVP. For the corresponding zinc oxide-modified composite, the amount of biofilm decreased significantly. The largest amount of bacterial biofilm was observed for composites containing no zinc oxide in the case of *S. aureus* strain. Almost the entire surface of the sample was stained red. In this case, the addition of zinc oxide also significantly reduced bacterial biofilm formation.

Summarizing, the ability of the composites presented in this article to inhibit biofilm is extremely important. This is because the removal of biofilm from various types of surfaces is extremely difficult. The mature form of a biofilm is characterized by the presence of many microcolonies, in which the cells of the organism are connected by an extracellular polymeric substance. This includes polysaccharides, proteins, nucleic acids or water, among others. The cells inside the biofilm are specialized to perform different functions, often with different characteristics to cells that live in free form. The construction, as well as the organization of these clusters, allows microorganisms to be protected from adverse external influences. The composites presented in this paper significantly reduced the ability of bacteria to form a biofilm on their surface. This was particularly evident in the case of *P. aeruginosa* and *E. coli* strains. Both the base composite and the zinc oxide-modified material practically

Table 10: Detection of bacterial survival rate in the presence of control-based and zinc oxide-modifying composites containing AEH, MMA, HEMA, and NVP as solvent using the method with TTC as a reaction substrate.

Microorganism/composite	*P. aeruginosa*	*E. coli*	*S. aureus*
Growth control	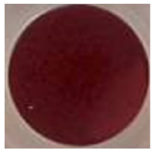		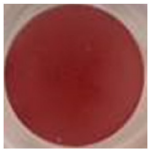
BPA.DM + AEH			
BPA.DM + AEH + 10 %ZnO			
BPA.DM + MMA			
BPA.DM + MMA + 10 %ZnO			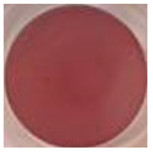
BPA.DM + HEMA			
BPA.DM + HEMA + 10 %ZnO			
BPA.DM + NVP		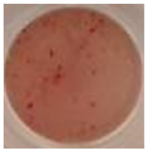	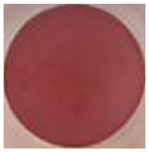
BPA.DM + NVP + 10 %ZnO			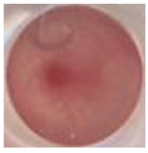

Table 11: Evaluation of the bacterial biofilm formation on the surface of control-based and zinc oxide-modified composites containing AEH, MMA, HEMA, and NVP as solvent using TTC as reaction substrate.

Microorganism/composite	*P. aeruginosa*	*E. coli*	*S. aureus*
BPA.DM + AEH	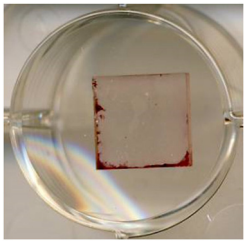	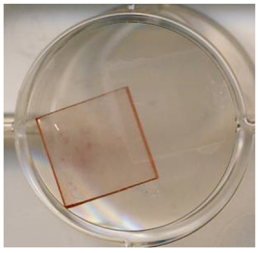	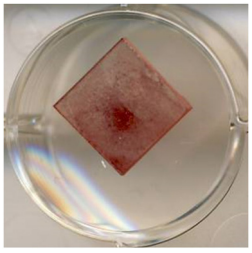
BPA.DM + AEH + 10 %ZnO	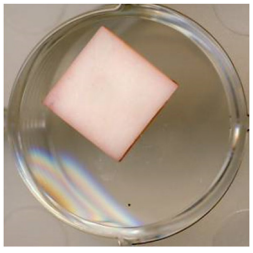	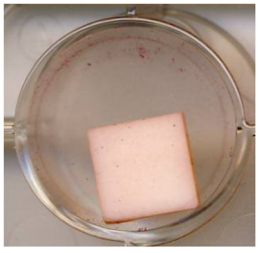	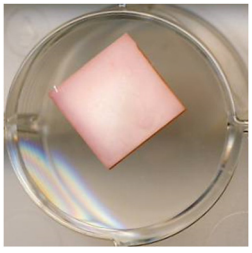
BPA.DM + MMA	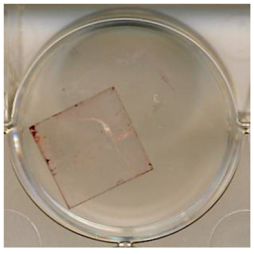	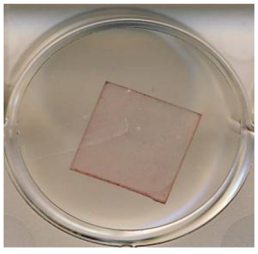	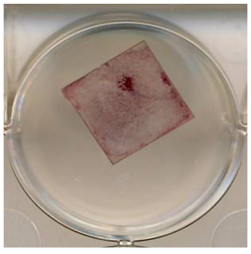
BPA.DM + MMA + 10 %ZnO	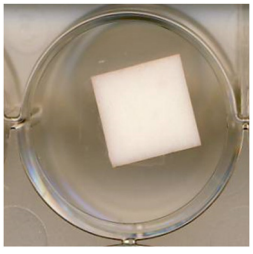	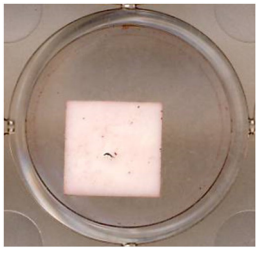	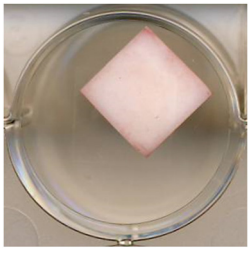
BPA.DM + HEMA	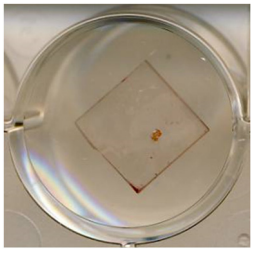	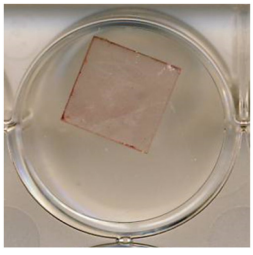	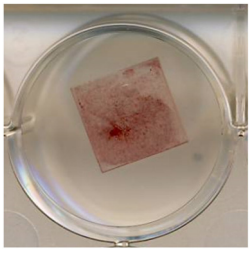
BPA.DM + HEMA + 10 %ZnO	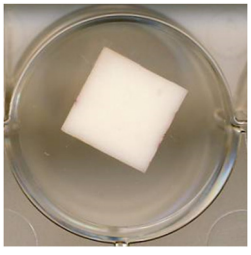	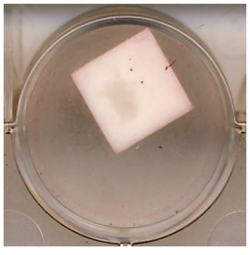	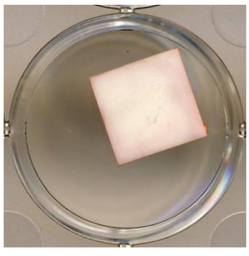

Table 11: (continued)

Microorganism/composite	*P. aeruginosa*	*E. coli*	*S. aureus*
BPA.DM + NVP	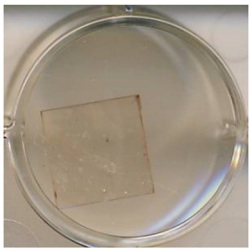	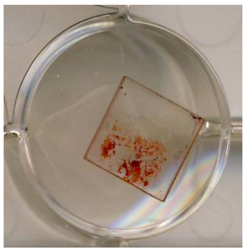	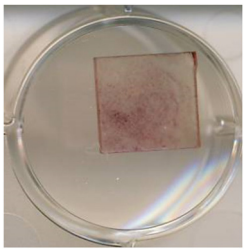
BPA.DM + NVP + 10 %ZnO	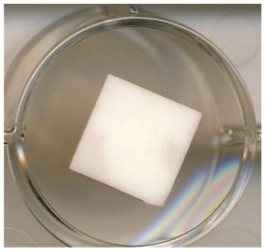	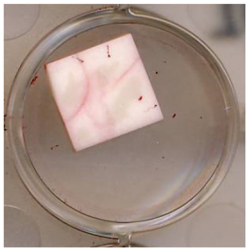	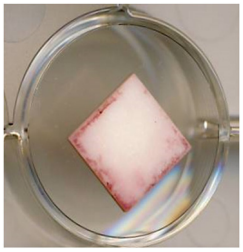

prevented biofilm formation, which was confirmed by the lack of red coloration resulting from the presence of formazan. For *S. aureus*, the base composites showed no ability to inhibit biofilm layer formation. In contrast, modification of these composites with zinc oxide resulted in the biofilm not being visible on their surface[52] indicated that modification of polyvinyl chloride films with ZnO nanoparticles results in an approximately 55 % reduction in biofilm formation concerning the control sample. They showed no significant difference between the percentage of zinc oxide and biofilm reduction[53] used composites containing nanosilver and chitosan. The most sensitive microorganism to the nanosilver-chitosan composite was *S. aureus*. In both the exponential and stationary growth phases, a high bactericidal effect and inhibition of biofilm formation was obtained. For *E. coli*, it was indicated that a greater inhibitory effect was seen in the logarithmic growth phase than in the stationary phase. Similar results were observed for *P. aeruginosa*. It has been confirmed that the higher the concentration of nanosilver in the composite material, the less bacterial biofilm formed on its surface,[54] as well as[55] indicated that modification of materials with silver ions should show strong bactericidal activity against *S. aureus*, *S. epidermidis*, *P. aeruginosa* and *E. coli*. They explain this by the fact that silver ions interact with cytoplasmic components and nucleic acids, which contributes to the inhibition of respiratory chain enzymes and disrupts membrane permeability. This also contributes to limiting the potential for biofilm formation[56] indicated that titanium dioxide-modified implants can significantly inhibit bacteria, fungi and also prevent biofilm formation on the implant surface. However, the activation of this compound only takes place after exposure to ultraviolet light. Such properties are of great importance for the potential use of composites as protective layers on the surfaces of objects in hospitals or public places.

As was mentioned previously, the mechanism of activity of zinc oxide against bacteria is not yet completely understood. Penetration and disorganization of the cell membrane, which consists of proteins and lipids, is indicated as one of the widely described potential mechanisms. This takes place upon contact with zinc oxide nanoparticles and leads to inhibition of bacterial growth. In addition, zinc ions have the ability to bind to the cell membranes of microorganisms. This results in a prolongation of the lag phase in the growth cycle of microorganisms.[57,58] This activity can be compared to antibiotics of the polymyxin group. They are part of the polypeptide group of antibiotics. Polymyxins B and E have been used in clinical applications. These factors have an effect on lipopolysaccharides which are important element of the outer membrane of the bacterial cell. As a consequence, the normal functioning of the bacterial cell is disrupted and cell death occurs. This confirms the bactericidal properties of polymyxins.[59,60] It is also hypothesized that polymyxins have the ability to induce the

uncontrolled formation and accumulation of hydroxyl radicals, which can damage DNA, lipids and also proteins.[61,62] The question is if such mechanisms can be attributed to the bactericidal properties of zinc oxide. While it is true that the chemical mechanism of the zinc oxide reaction may be different, the action on the protein-lipid membrane of the bacterial cell appears to be the same.

Conclusions

In conclusion, it can be said that the proposed new composites based on the methacrylates modified with the addition of zinc oxide seem to be a good proposal of materials for widely practical applications. Their technical parameters meet the requirements for this type of polymers and the addition of a component with documented antimicrobial activity greatly expand the possibility of their application in both industry and biomedicine.

Research ethics: Not applicable.
Informed consent: Not applicable.
Author contributions: KM – conceptualization, data curation, formal analysis, investigation, methodology, writing – original draft, writing – rewiev and editing, BP – conceptualization, methodology, writing – rewiev and editing, KSz – methodology, formal analysis, writing – rewiev and editing, MO-J -methodology, formal analysis, writing – rewiev and editing, MJ – conceptualization, formal analysis, methodology, writing – rewiev and editing, All authors have accepted responsibility for the entire content of this manuscript and approved its submission.
Use of Large Language Models, AI and Machine Learning Tools: None declared.
Conflict of interest: The authors state no conflict of interest.
Research funding: None declared.
Data availability: Not applicable.
Patents: The research presented in the publication was reported in a patent application dated 15/03/2023. P.444108, “Method of obtaining a polymeric composite with antimicrobial activity and a polymeric composite obtained by this method”.

References

1. Allahverdiyev, A. M.; Abamor, E. S.; Bagirova, M.; Rafailovich, M. Antimicrobial Effects of TiO(2) and Ag(2)O Nanoparticles Against drug-resistant Bacteria and Leishmania Parasites. *Future Microbiol.* **2011**, *6*, 933–940. https://doi.org/10.2217/fmb.11.78.
2. Song, F.; Koo, H.; Ren, D. Effects of Material Properties on Bacterial Adhesion and Biofilm Formation. *J. Dent. Res*. **2015**, *94*, 1027–1034. https://doi.org/10.1177/0022034515587690.
3. Foxman, B.; Salzman, E.; Gesierich, C.; Gardner, S.; Ammerman, M.; Eisenberg, M.; Wigginton, K. Wastewater Surveillance of antibiotic-resistant Bacteria for Public Health Action: Potential and Challenges. *Am. J. Epidemiol.* **2025**, *194*, 1192–1199. https://doi.org/10.1093/aje/kwae419.
4. Galgano, M.; Pellegrini, F.; Catalano, E.; Capozzi, L.; Del Sambro, L.; Sposato, A.; Lucente, M. S.; Vasinioti, V. I.; Catella, C.; Odigie, A. E.; Tempesta, M.; Pratelli, A.; Capozza, P. Acquired Bacterial Resistance to Antibiotics and Resistance Genes: From past to Future. *Antibiotics* **2025**, *14*, 222. https://doi.org/10.3390/antibiotics14030222.
5. Karnwal, A.; Jassim, A. Y.; Mohammed, A. A.; Al-Tawaha, A. R. M. S.; Selvaraj, M.; Malik, T. Addressing the Global Challenge of Bacterial Drug Resistance: Insights, Strategies, and Future Directions. *Front. Microbiol*. **2025**, *16*. https://doi.org/10.3389/fmicb.2025.1517772.
6. Teymouri, S.; Yousefi, M. H.; Heidari, S.; Farokhi, S.; Afkhami, H.; Kashfi, M. Beyond Antibiotics: Mesenchymal Stem Cells and bacteriophages-new Approaches to Combat Bacterial Resistance in Wound Infections. *Mol. Biol. Rep*. **2025**, *52*, 64. https://doi.org/10.1007/s11033-024-10163-x.
7. Baptista, P. V.; McCusker, M. P.; Carvalho, A.; Ferreira, D. A.; Mohan, N. M.; Martins, M.; Fernandes, A. R. Nano-Strategies to Fight Multidrug Resistant bacteria-“A Battle of the Titans”. *Front. Microbiol*. **2018**, *9*. https://doi.org/10.3389/fmicb.2018.01441.
8. Herman, A.; Herman, A. P. Nanoparticles as Antimicrobial Agents: Their Toxicity and Mechanisms of Action. *J. Nanosci. Nanotechnol*. **2014**, *14*, 946–957. https://doi.org/10.1166/jnn.2014.9054.
9. Lithi, I. J.; Ahmed Nakib, K. I.; Chowdhury, A. M. S.; Sahadat Hossain, Md. A Review on the Green Synthesis of Metal (Ag, Cu, and Au) and Metal Oxide (Zno, MgO, Co_3O_4, and TiO_2) Nanoparticles Using Plant Extracts for Developing Antimicrobial Properties. *Nanoscale Adv.* **2025**, *7*, 2446–2473. https://doi.org/10.1039/D5NA00037H.

10. Mohammed, A. M.; Mohammed, M.; Oleiwi, J. K.; Ihmedee, F. H.; Adam, T.; Betar, B. O.; Gopinath, S. C. B. The Anticancer, Antioxidant, and Antimicrobial Properties of Zinc Oxide Nanoparticles: A Comprehensive Review. *Nano TransMed.* **2025**, *4*, 100097. https://doi.org/10.1016/j.ntm.2025.100097.
11. Buzea, C.; Pacheco, I. I.; Robbie, K. Nanomaterials and Nanoparticles: Sources and Toxicity. *Biointerphases* **2007**, *2*, MR17–MR71. https://doi.org/10.1116/1.2815690.
12. Darini, R.; Ahari, H.; Khosrojerdi, A.; Jannat, B.; Babazadeh, H. Antimicrobial Properties of Graphene Sheets Embedded with Titanium Oxide and Calcium Oxide Nanoparticles for Industrial Wastewater Treatment. *Sci. Rep*. **2025**, *15*, 1007. https://doi.org/10.1038/s41598-024-84335-x.
13. Demirbas, A.; Karsli, B. Innovative chitosan-silver Nanoparticles: Green Synthesis, Antimicrobial Properties, and Migration Assessment for Food Packaging. *Food Chem*. **2025**, *467*, 142363. https://doi.org/10.1016/j.foodchem.2024.142363.
14. Karuppan Perumal, M. K.; Rajasekaran, M. B. S.; Rajan Renuka, R.; Samrot, A. V.; Nagarajan, M. Zinc Oxide Nanoparticles and Their Nanocomposites as an Imperative Coating for Smart Food Packaging. *Appl. Food Res.* **2025**, *5*, 100849. https://doi.org/10.1016/j.afres.2025.100849.
15. Pal, S.; Tak, Y. K.; Song, J. M. Does the Antibacterial Activity of Silver Nanoparticles Depend on the Shape of the Nanoparticle? A Study of the Gram-negative Bacterium *Escherichia coli*. *Appl. Environ. Microbiol*. **2007**, *73*, 1712–1720. https://doi.org/10.1128/AEM.02218-06.
16. Fang, X.; Yu, R.; Li, B.; Somasundaran, P.; Chandran, K. Stresses Exerted by ZnO, CeO_2 and Anatase TiO_2 Nanoparticles on the Nitrosomonas europaea. *J. Colloid Interface Sci*. **2010**, *348*, 329–334. https://doi.org/10.1016/j.jcis.2010.04.075.
17. Franklin, N. M.; Rogers, N. J.; Apte, S. C.; Batley, G. E.; Gadd, G. E.; Casey, P. S. Comparative Toxicity of Nanoparticulate ZnO, Bulk ZnO, and $ZnCl_2$ to a Freshwater Microalga (Pseudokirchneriella Subcapitata): the Importance of Particle Solubility. *Environ. Sci. Technol*. **2007**, *41*, 8484–8490. https://doi.org/10.1021/es071445r.
18. Lipovsky, A.; Nitzan, Y.; Gedanken, A.; Lubart, R. Antifungal Activity of ZnO nanoparticles-the Role of ROS Mediated Cell Injury. *Nanotechnology* **2011**, *22*. https://doi.org/10.1088/0957-4484/22/10/105101.
19. Martorano, L. M.; Stork, C. J.; Li, Y. V. UV irradiation-induced Zinc Dissociation from Commercial Zinc Oxide Sunscreen and its Action in Human Epidermal Keratinocytes. *J. Cosmet. Dermatol.* **2010**, *9*, 276–286. https://doi.org/10.1111/j.1473-2165.2010.00521.x.
20. Zhang, L.; Jiang, Y.; Ding, Y.; Daskalakis, N.; Jeuken, L.; Povey, M.; O'Neill, A. J.; York, D. W. Mechanistic Investigation into Antibacterial Behaviour of Suspensions of ZnO Nanoparticles Against *E. coli*. *J. Nanopart. Res.* **2010**, *12*, 1625–1636. https://doi.org/10.1007/s11051-009-9711-1.
21. Jones, N.; Ray, B.; Ranjit, K. T.; Manna, A. C. Antibacterial Activity of ZnO Nanoparticle Suspensions on a Broad Spectrum of Microorganisms. *FEMS Microbiol. Lett*. **2008**, *279*, 71–76. https://doi.org/10.1111/j.1574-6968.2007.01012.x.
22. Khan, M. F.; Ansari, A. H.; Hameedullah, M.; Ahmad, E.; Husain, F. M.; Zia, Q.; Baig, U.; Zaheer, M. R.; Alam, M. M.; Khan, A. M.; AlOthman, Z. A.; Ahmad, I.; Ashraf, G. M.; Aliev, G. Sol-Gel Synthesis of Thorn-like ZnO Nanoparticles Endorsing Mechanical Stirring Effect and Their Antimicrobial Activities: Potential Role as nano-Antibiotics. *Sci. Rep*. **2016**, *6*. https://doi.org/10.1038/srep27689.
23. Liu, J.; Feng, X.; Wei, L.; Chen, L.; Song, B.; Shao, L. The Toxicology of ion-shedding Zinc Oxide Nanoparticles. *Crit. Rev. Toxicol*. **2016**, *46*, 348–384. https://doi.org/10.3109/10408444.2015.1137864.
24. Premanathan, M.; Karthikeyan, K.; Jeyasubramanian, K.; Manivannan, G. Selective Toxicity of ZnO Nanoparticles Toward Gram-positive Bacteria and Cancer Cells by Apoptosis Through Lipid Peroxidation. *Nanomedicine* **2011**, *7*, 184–192. https://doi.org/10.1016/j.nano.2010.10.001.
25. Wang, H.; Wingett, D.; Engelhard, M. H.; Feris, K.; Reddy, K. M.; Turner, P.; Layne, J.; Hanley, C.; Bell, J.; Tenne, D.; Wang, C.; Punnoose, A. Fluorescent Dye Encapsulated ZnO Particles with Cell-specific Toxicity for Potential Use in Biomedical Applications. *J. Mater. Sci. Mater. Med.* **2009**, *20*, 11–22. https://doi.org/10.1007/s10856-008-3541-z.
26. Applerot, G.; Lipovsky, A.; Dror, R.; Perkas, N.; Nitzan, Y.; Lubart, R.; Gedanken, A. Enhanced Antibacterial Activity of Nanocrystalline ZnO due to Increased Ros-Mediated Cell Injury. *Adv. Funct. Mater*. **2009**, *19*, 842–852. https://doi.org/10.1002/adfm.200801081.
27. Sawai, J.; Shoji, S.; Igarashi, H.; Hashimoto, A.; Kokugan, T.; Shimizu, M.; Kojima, H. Hydrogen Peroxide as an Antibacterial Factor in Zinc Oxide Powder Slurry. *J. Ferment. Bioeng*. **1998**, *86*, 521–522. https://doi.org/10.1016/S0922-338X(98)80165-7.
28. Brayner, R.; Ferrari-Iliou, R.; Brivois, N.; Djediat, S.; Benedetti, M. F.; Fiévet, F. Toxicological Impact Studies Based on *Escherichia coli* Bacteria in Ultrafine ZnO Nanoparticles Colloidal Medium. *Nano Lett*. **2006**, *6*, 866–870. https://doi.org/10.1021/nl052326h.
29. Jiang, W.; Mashayekhi, H.; Xing, B. Bacterial Toxicity Comparison Between nano- and Micro-scaled Oxide Particles. *Environ. Pollut.* **2009**, *157*, 1619–1625. https://doi.org/10.1016/j.envpol.2008.12.025.
30. Brunner, T. J.; Wick, P.; Manser, P.; Spohn, P.; Grass, R. N.; Limbach, L. K.; Bruinink, A.; Stark, W. J. In Vitro Cytotoxicity of Oxide Nanoparticles: Comparison to Asbestos, Silica, and the Effect of Particle Solubility. *Environ. Sci. Technol*. **2006**, *40*, 4374–4381. https://doi.org/10.1021/es052069i.
31. Li, M.; Zhu, L.; Lin, D. Toxicity of ZnO Nanoparticles to Escherichia Coli: Mechanism and the Influence of Medium Components. *Environ. Sci. Technol*. **2011**, *45*, 1977–1983. https://doi.org/10.1021/es102624t.
32. Lange, R. S. Holly und P. Sohár: Absorption Spectra in the Infrared Region, Theoretical and Technical Introduction. 183 Seiten, Zahlreiche Tab. Akadémiai Kiadó, Budapest 1975. *Food / Nahrung* **1976**, *20*, 861–862. https://doi.org/10.1002/food.19760200828.
33. Oliveira, A.; Cabral, L. M. C.; Bizzo, H.; Arruda, N. P.; Freitas, S. P. Identification and Recovery of Volatiles Organic Compounds (VOCs) in the Coffee-Producing Wastewater. *J. Water Resour. Prot.* **2014**, *06*, 375–380. https://doi.org/10.4236/jwarp.2014.64039.
34. Wnuczek, K.; Puszka, A.; Klapiszewski, Ł.; Podkościelna, B. Preparation, Thermal, and Thermo-Mechanical Characterization of Polymeric Blends Based on Di(Meth)Acrylate Monomers. *Polymers (Basel)* **2021**, *13*. https://doi.org/10.3390/polym13060878.

35. Młynarczyk, K.; Podkościelna, B.; Jaszek, M.; Osińska-Jaroszuk, M. Badania Stabilności Termicznej i Potencjału Przeciwdrobnoustrojowego Kompozytów Zawierających Modyfikatory Nieorganiczne. In *Nauka i Przemysł – Lubelskie Spotkania Studenckie*; Kołodyńska, D., Ed.; Uniwersytet Marii Curie-Skłodowskiej w Lublinie: Lublin, 2024; pp. 70–73.
36. Młynarczyk, K.; Podkościelna, B.; Jaszek, M.; Osińska-Jaroszuk, M. Badania Właściwości Kompozytów Opartych Na Pochodnych Akrylanu Z Dodatkiem N-winylopirolidonu. In *Nauka i Przemysł – Lubelskie Spotkania Studenckie*; Kołodyńska, D., Ed.; Uniwerstet Marii Curie-Skłodowskiej w Lublinie: Lublin, 2023b; pp. 294–297.
37. Ijaz, M.; Zafar, M.; Islam, A.; Afsheen, S.; Iqbal, T. A Review on Antibacterial Properties of Biologically Synthesized Zinc Oxide Nanostructures. *J. Inorg. Organomet. Polym. Mater*. **2020**, *30*, 2815–2826. https://doi.org/10.1007/s10904-020-01603-9.
38. Król, A.; Pomastowski, P.; Rafińska, K.; Railean-Plugaru, V.; Buszewski, B. Zinc Oxide Nanoparticles: Synthesis, Antiseptic Activity and Toxicity Mechanism. *Adv. Colloid Interface Sci*. **2017**, *249*, 37–52. https://doi.org/10.1016/J.CIS.2017.07.033.
39. Kyomuhimbo, H. D.; Michira, I. N.; Mwaura, F. B.; Derese, S.; Feleni, U.; Iwuoha, E. I. Silver–Zinc Oxide Nanocomposite Antiseptic from the Extract of Bidens pilosa. *SN Appl. Sci.* **2019**, *1*, 681. https://doi.org/10.1007/s42452-019-0722-y.
40. Młynarczyk, K.; Jaszek, M.; Osińska-Jaroszuk, M.; Podkościelna, B. Synthesis, Aging and Antimicrobial Tests of (Di)Acrylate Composites. *Pure Appl. Chem.* **2023a**, *95*, 611–629. https://doi.org/10.1515/pac-2023-0109.
41. Gunalan, S.; Sivaraj, R.; Rajendran, V. Green Synthesized ZnO Nanoparticles Against Bacterial and Fungal Pathogens. *Prog. Nat. Sci.: Mater. Int.* **2012**, *22*, 693–700. https://doi.org/10.1016/J.PNSC.2012.11.015.
42. Bharathi, D.; Ranjithkumar, R.; Chandarshekar, B.; Bhuvaneshwari, V. Preparation of Chitosan Coated Zinc Oxide Nanocomposite for Enhanced Antibacterial and Photocatalytic Activity: as a Bionanocomposite. *Int. J. Biol. Macromol*. **2019**, *129*, 989–996. https://doi.org/10.1016/J.IJBIOMAC.2019.02.061.
43. Cheknev, S. B.; Babaeva, E. E.; Golub, A. E.; Denisova, E. A.; Vorobieva, U. A. The Effects of Copper and Zinc Ions During Their Binding with Human Serum γ-Globulin. *Med. Immunol. (Russia)* **2014**, *8*, 615. https://doi.org/10.15789/1563-0625-2006-5-6-615-622.
44. Ibrahem, E. J.; Yasin, Y. S.; Jasim, O. K. Antibacterial Activity of Zinc Oxide Nanoparticles Against Staphylococcus aureus and Pseudomonas aeruginosa Isolated from Burn Wound Infections. *Cihan University-Erbil Sci. J.* **2017**, *2017*, 265–277. https://doi.org/10.24086/cuesj.si.2017.n2a24.
45. M Yousef, J.; N Danial, E. In *Vitro* Antibacterial Activity and Minimum Inhibitory Concentration of Zinc Oxide and Nano-particle Zinc Oxide Against Pathogenic Strains. *Int. J. Health Sci.* **2012**, *2*, 38–42. https://doi.org/10.5923/j.health.20120204.04.J., N.
46. Chitra, C.; Kumar, D.; Shakti, L.; Diana, S.; Balaji, V. Technical and Interpretative Issues of Fosfomycin Susceptibility Testing. *Indian J. Med. Microbiol.* **2015**, *33*, 611–612. https://doi.org/10.4103/0255-0857.167338.
47. Li, X.; Xing, Y.; Jiang, Y.; Ding, Y.; Li, W. Antimicrobial Activities of ZnO Powder-Coated PVC Film to Inactivate Food Pathogens. *Int. J. Food Sci. Technol*. **2009**, *44*, 2161–2168. https://doi.org/10.1111/j.1365-2621.2009.02055.x.
48. Reddy, L. S.; Nisha, M. M.; Joice, M.; Shilpa, P. N. Antimicrobial Activity of Zinc Oxide (ZnO) Nanoparticle Against *Klebsiella pneumoniae*. *Pharm. Biol.* **2014**, *52*, 1388–1397. https://doi.org/10.3109/13880209.2014.893001.
49. Brown, H. L.; van Vliet, A. H. M.; Betts, R. P.; Reuter, M. Tetrazolium Reduction Allows Assessment of Biofilm Formation by *Campylobacter jejuni* in a Food Matrix Model. *J. Appl. Microbiol.* **2013**, *115*, 1212–1221. https://doi.org/10.1111/jam.12316.
50. Farouk, F.; Kabil, F. Zinc Oxide Chitosan nano-composite Membrane for Enhancing Transplants Production in Strawberry Nurseries via Targeting Chitin Elicitor Receptor Kinase. *Int. Nano Lett.* **2022**, *12*, 301–312. https://doi.org/10.1007/s40089-022-00374-0.
51. Moussa, S. H.; Tayel, A. A.; Al-Hassan, A. A.; Farouk, A. Tetrazolium/Formazan Test as an Efficient Method to Determine Fungal Chitosan Antimicrobial Activity. *J. Mycol.* **2013**, *2013*, 1–7. https://doi.org/10.1155/2013/753692.
52. Seil, J. T.; Webster, T. J. Antibacterial Zinc Oxide Nanoparticles in Polymer Biomaterial Composites. *MRS Proc.* **2011**, *1316*. mrsf10-1316-qq12-29 https://doi.org/10.1557/opl.2011.667.
53. Regiel-Futyra, A.; Kus-Liśkiewicz, M.; Sebastian, V.; Irusta, S.; Arruebo, M.; Kyzioł, A.; Stochel, G. Development of Noncytotoxic silver–chitosan Nanocomposites for Efficient Control of Biofilm Forming Microbes. *RSC Adv*. **2017**, *7*, 52398–52413. https://doi.org/10.1039/C7RA08359A.
54. Birla, S. S.; Tiwari, V. V.; Gade, A. K.; Ingle, A. P.; Yadav, A. P.; Rai, M. K. Fabrication of Silver Nanoparticles by *Phoma glomerata* and its Combined Effect Against *Escherichia coli*, *Pseudomonas aeruginosa* and *Staphylococcus aureus*. *Lett. Appl. Microbiol*. **2009**, *48*, 173–179. https://doi.org/10.1111/j.1472-765X.2008.02510.x.
55. Rai, M.; Yadav, A.; Gade, A. Silver Nanoparticles as a New Generation of Antimicrobials. *Biotechnol. Adv*. **2009**, *27*, 76–83. https://doi.org/10.1016/j.biotechadv.2008.09.002.
56. Ditta, I. B.; Steele, A.; Liptrot, C.; Tobin, J.; Tyler, H.; Yates, H. M.; Sheel, D. W.; Foster, H. A. Photocatalytic Antimicrobial Activity of Thin Surface Films of TiO2, CuO and TiO2/CuO Dual Layers on Escherichia coli and Bacteriophage T4. *Appl. Microbiol. Biotechnol*. **2008**, *79*, 127–133. https://doi.org/10.1007/s00253-008-1411-8.
57. Li, Q.; Mahendra, S.; Lyon, D. Y.; Brunet, L.; Liga, M. V.; Li, D.; Alvarez, P. J. J. Antimicrobial Nanomaterials for Water Disinfection and Microbial Control: Potential Applications and Implications. *Water Res*. **2008**, *42*, 4591–4602. https://doi.org/10.1016/j.watres.2008.08.015.
58. Seil, J. T.; Webster, T. J. Antibacterial Effect of Zinc Oxide Nanoparticles Combined with Ultrasound. *Nanotechnology* **2012**, *23*. https://doi.org/10.1088/0957-4484/23/49/495101.
59. Humphries, R. M.; Kelesidis, T.; Dien Bard, J.; Ward, K. W.; Bhattacharya, D.; Lewinski, M. A. Successful Treatment of pan-resistant Klebsiella pneumoniae Pneumonia and Bacteraemia with a Combination of high-dose Tigecycline and Colistin. *J. Med. Microbiol*. **2010**, *59*, 1383–1386. https://doi.org/10.1099/jmm.0.023010-0.

60. Michalopoulos, A.; Falagas, M. E. Colistin and Polymyxin B in Critical Care. *Crit. Care Clin.* **2008**, *24*, 377–391. https://doi.org/10.1016/j.ccc.2007.12.003.
61. Falagas, M. E.; Kasiakou, S. K.; Saravolatz, L. D. Colistin: the Revival of Polymyxins for the Management of multidrug-resistant Gram-negative Bacterial Infections. *Clin. Infect. Dis.* **2005**, *40*, 1333–1341. https://doi.org/10.1086/429323.
62. Yu, Z.; Qin, W.; Lin, J.; Fang, S.; Qiu, J. Antibacterial Mechanisms of Polymyxin and Bacterial Resistance. *Biomed. Res. Int.* **2015**, *2015*. https://doi.org/10.1155/2015/679109.